Hydraulic Performance of Composite-Type Seawalls Applied in Malaysia

by

Nabilah Ab. Qahar

Dissertation submitted in partial fulfilment of

the requirements for the

Bachelor of Engineering (Hons)

(Civil Engineering)

DECEMBER 2007

Universiti Teknologi PETRONAS
Bandar Seri Iskandar
31750 Tronoh
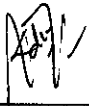Perak Darul Ridzuan

CERTIFICATION OF APPROVAL

Hydraulic Performance of Composite Seawalls Applied in Malaysia

by

Nabilah Ab. Qahar

A project dissertation submitted to the
Civil Engineering Programme
Universiti Teknologi PETRONAS
in partial fulfilment of the requirement for the
BACHELOR OF ENGINEERING (Hons)
(CIVIL ENGINEERING)

Approved by,

_____
(Mr. Teh Hee Min)

UNIVERSITI TEKNOLOGI PETRONAS

TRONOH, PERAK

December 2007

CERTIFICATION OF ORIGINALITY

This is to certify that I am responsible for the work submitted in this project, that the original work is my own except as specified in the references and acknowledgements, and that the original work contained herein have not been undertaken or done by unspecified sources or persons.

NABILAH AB. QAHAR

ABSTRACT

This is a report on the Final Year Project titled 'Hydraulic Performance of Composite-Type Seawalls Applied in Malaysia'. Composite-type seawalls were stacked armour stones or wave dissipating blocks fronting the vertical seawalls to reduce waves overtopping. Under certain weather condition and storm action in Malaysia, waves overtopping would be frequent and violent where hinterlands are prone to the risk of flooding and damaged to infrastructures. The objectives of this project were to study the existing types of composite seawalls applied in Malaysia and conduct risk assessment on the selected composite seawalls. Three models are fabricated which were concrete block, composite seawalls using quarrystones and concrete cubes as armour units. The models were constructed on a scale of 1:15 using concrete mortar. Tests were conducted in a flap-type wave generator in the UTP Hydraulic Engineering Laboratory. First part of the project only highlights two preliminary tests which were the determination of wave period, T with respect to frequency, f and determination of incident wave height, H_i with respect to wave period, T in four different water depths (18, 20, 22 and 24 cm). The results were used in the second part of the project which was the determination of overtopping rates, q for three different models of seawalls for $d = 18, 20, 22$ and 24 cm. The overtopping rates were then analyzed with respect to wave steepness, H_i/gT^2 and incident wave height, H_i. It is founded that q increased as H_i and d increased. Then risk assessment on pedestrians, vehicles, buildings and embankment seawalls are made. The tolerable overtopping rates developed by Owen (1994) are used as guidelines to the assessment. Observed from the assessment, the waves overtopping values were hazardous to pedestrians, vehicles and buildings. As for embankment seawalls, the values cause no damage. It is concluded that overtopping rates are influenced by H_i and d while further research can be done in order to minimize the hazards to pedestrians, vehicles and buildings.

ACKNOWLEDGEMENT

This research and dissertation would never have been able to finish without the guidance of my supervisor, help from technicians, and support from my friends.

Foremost, I would like to express my deepest gratitude to my supervisor, Mr. Teh Hee Min, for his excellent guidance, caring and patience. I also would like to thank Prof. Malay Chaudari as my co-supervisor, who patiently corrected my writing and morally supported my research.

Special thanks goes to Ir. Nor Hisham M Ghazali for Department of Irrigation and Drainage Malaysia, who was willing to share useful information regarding the research.

Many thanks to Mr. Idris, Mr. Meor Asniwan, Mr. Mohd Zaini Hashim and Mr. Johan Ariff Mohamad, the lab technicians for helping me during the lab sessions. Sincere gratitude is also extended to the groups of students assigned by my supervisor to help speed-up the lab sessions. My research would not have been possible without all the helps.

Lastly, I should thank many individuals, friends and colleagues who have not been mentioned here personally in making this educational process a success. May be I could not have made it without your supports.

TABLE OF CONTENTS

LIST OF FIGURES

LIST OF TABLES

CHAPTER 1

INTRODUCTION

1.1   BACKGROUND OF STUDY

Seawalls are the most common form of coastal defense and most generally regarded by the public as representing the best form. It is because by representing a physical barrier between land and sea, they prevent any erosion of the hinterland and protect it from flooding. In addition, because they are such a solid barrier, the perceived level of protection from the sea is greater than many other forms of defense.

In the early days, seawalls were in the form of simple earth structures only to stop the sea flooding the land. Erosion was not taken into consideration. However, as the coastal development progressed, a vertical wall originally considered the best way to stop sea flooding and prevent erosion. Their use is worldwide and they are found on a range of coastal types.

Obviously, seawalls need to resist waves but they cannot withstand the forces by relying on the vertical walls or caissons itself. Therefore, it is a common practice to stack armour stones or wave dissipating blocks in front of the caisson for the purpose of wave energy dissipation and reduction of wave overtopping. Such a seawall is called "Composite-type Seawall".

1.2   PROBLEM STATEMENT

Since Malaysia is surrounded by sea, it is possible to have composite-type seawalls in several areas of interest to protect the hinterland from wave attack. However, seawalls only reduce wave overtopping. Under certain weather condition and storm action in Malaysia, wave overtopped the crest of the seawalls would be frequent and violent. Thus, hinterlands are prone to the risk of flooding and subsequent damage to infrastructures.

In order to minimize the associated risks, analytical and laboratory studies, and field tests need to be conducted.

1.3   OBJECTIVES OF STUDY

Upon completing the project, a few objectives need to be achieved. The objectives of study are as follows:

1. To identify and study the existing type of composite seawalls applied in Malaysia.

2. To construct several composite-type seawall models using proper materials according to selected type of composite seawalls.

3. To experimentally investigate the hydraulic performance of the selected composite-type seawalls.

4. To conduct risk assessment on the selected composite-type seawalls.

1.4 SCOPE OF STUDY

The study is divided into 5 major parts as follows:

1. Literature Review

In the literature review stage, existing designs of composite-type seawalls in Malaysia are referred to and identified. Wave overtopping estimation method, wave force characteristics, caisson stability and wave dissipating blocks against waves investigated by other researches are the important highlights to be studied during this stage.

2. Modeling

After identifying the composite-type seawalls in Malaysia, two designs will be selected for modeling purposes. The models on a suitable scale and specification will be used in laboratory tests.

3. Laboratory Set Up

Tools and equipment to be used will be identified and familiarized prior to the laboratory tests to avoid malfunctioning of the system. Accuracy of equipments used in the tests also will be checked in order to get accurate results.

4. Laboratory Tests

A series of laboratory tests on the models will be performed in the wave flume with varying water depth, wave height and wave period to determine wave overtopping and wave characteristics.

5. Analysis of Results

Results obtained from the laboratory tests will be analyzed and interpreted. The risk assessment for each model will be conducted according to the laboratory tests results.

CHAPTER 2

LITERATURE REVIEW

2.1   INTRODUCTION

This chapter describes and illustrates each of the main types of composite seawalls. The features of each type are briefly discussed. It also discusses the hydraulic responses such as wave run-up and wave overtopping. Besides, this chapter summarizes different analysis methods from a wide range sources.

2.2   TYPES OF COMPOSITE SEAWALLS

US Army Corps of Engineers classified composite seawalls according to geotechnical consideration as well as hydraulics factor. The geotechnical and hydraulics factor are essential in determining toe apron width. In these cases by considering geotechnical factor, the toe apron should be wider than the product of the effective embedment depth and the coefficient of passive earth pressure for the soil. However by using hydraulic considerations, the toe apron should be at least twice the incident wave height for sheet-pile walls and equal to the incident wave height for gravity walls. In addition, the apron should be at least 40 percent of the depth at the structure, d_s (Figure 2.1). Greatest width predicted by these geotechnical and hydraulic factors should be used for design.
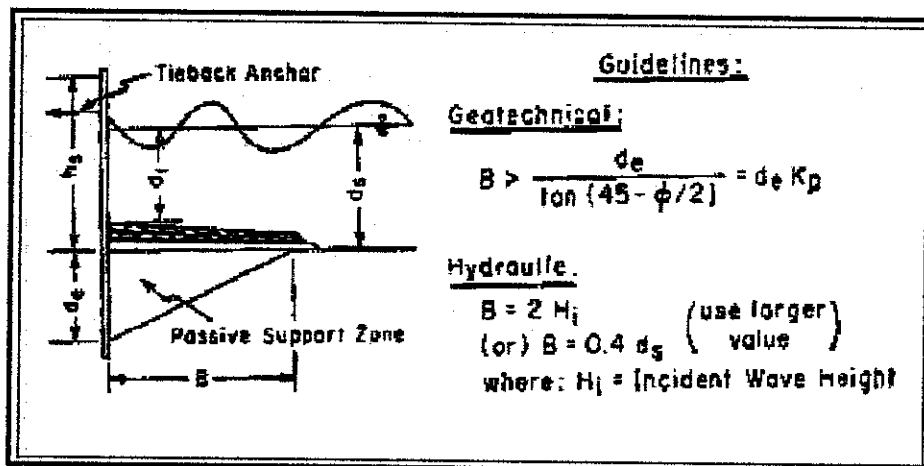
Figure 2.1: Toe aprons for sheet-pile bulkheads

Design consideration also focused on the seepage forces and the weight of toe stone. The hydraulic gradients of seepage flows under vertical walls can increase toe scour. Steep exit gradients reduce the net effective weight of the soil, making sediment movement under waves and currents more likely. This seepage flow may originate from general groundwater conditions, water derived from wave overtopping of the structure, or from precipitation. The following paragraphs are the configuration for composite seawalls and its figures.

2.2.1 Vertical Wall with Rock Toe
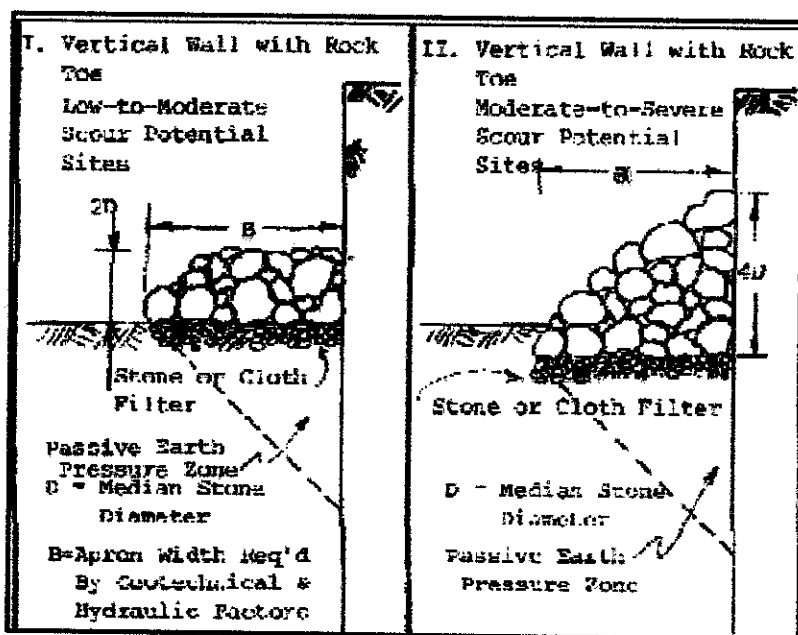
Figure 2.2: Vertical wall with rock toe

Common type of composite seawalls is vertical wall with rock toe. It consists of vertical wall and rocks as the armour units. The placement of rocks is according to the site scour potential. The left hand side picture in Figure 2.2 shows rocks placement for low to moderate scour potential sites which the height of armour units is two times the median rock diameter. The shape of the armour units is trapezoidal compare to the second picture which is triangular. The triangular armour unit's placement is for moderate to severe scour potential sites with height of four times the median rock diameter.

2.2.2 Vertical Wall with Gabion Toe
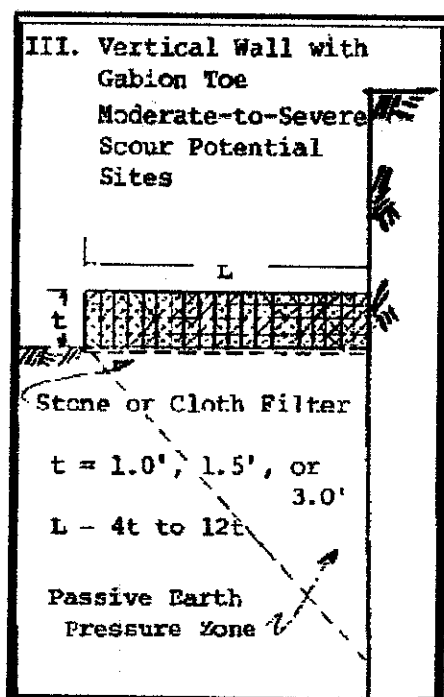
Figure 2.3: Vertical wall with Gabion toe

The other type of composite seawall is vertical wall with Gabion toe as shown in Figure 2.3. A unit of Gabion is a steel wire basket filled with stones. It can be arranged together by stacking vertically or stepped up a slope to conform to ground movement, dissipate energy from flowing water and drain freely. According to the manual, this type of composite seawall is suitable for moderate to severe scour potential sites.

2.2.3 Vertical Wall with Lean Cement-Filled Bag Toe
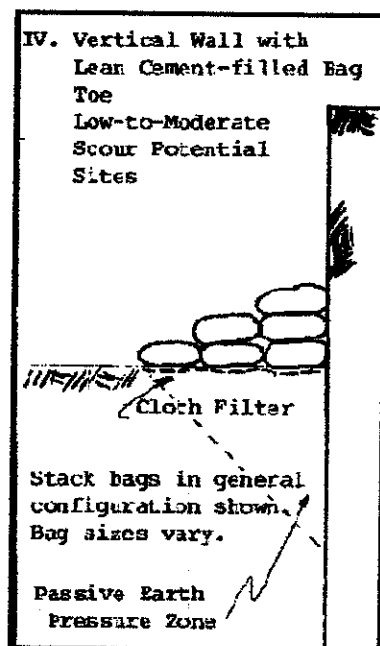
Figure 2.4: Vertical wall with lean cement-filled bag toe

Figure 2.4 shows another alternative for composite seawall which use lean cement-filled bag as the armour units. The bags were filled with concrete or sand and stacked on each other to form a slope. The bags size varies with requirement and suitable for low to moderate scour potential sites.

2.3 WAVE PROCESSES

In order to conduct the physical tests, further understanding regarding the wave processes is necessary. The two main wave processes involve in this research are wave run-up and wave overtopping.

2.3.1 Wave Run-up

Wave action on a structure will cause the water surface to oscillate over a vertical range generally greater than the incident wave height. The extreme high level reached by

waves on a structure is the wave run-up. It is the vertical height above the still water level to which water from an incident wave will run up the face of the structure. In case of vertical structures, the run-up height is that of the crest of standing waves in front of them. The run-up level can be used to assess the required level of the crest of the structure or as an indicator of the occurrence of wave overtopping. For design purpose, the amount of wave run-up is often indicated by $R_{u2\%}$, and is defined as the run-up level, vertically measured with respect to the adjusted still water level (SWL), which is exceeded by 2 % of the incident waves. Over most wave conditions and slopes, a rubble slope will dissipate more wave energy and result in fewer run-ups than a smooth or non-porous slope does. This reduction is influenced by the permeability of the armour, filter and underlayers, and by the steepness and period of the waves.

The relative run-up is given by $R_{u2\%} / H_s$, with H_s the significant wave height, being the average value of the highest 1/3 part of the wave heights, or the wave height based on energy: $4\sqrt{m_0}$, with m_0 the zeroth moment of the energy density spectrum. This H_s is the significant wave height at the toe of the structure. The relative run-up is usually given as a function of the surf similarity parameter or breaker parameter which is defined as

$$\xi_{op} = \tan \alpha / \sqrt{s_{op}} \qquad\qquad \text{(Eqn 2.1)}$$

where, ξ_{op} = the breaker parameter,

α = the average slope angle, and

s_{op} = the wave steepness = $2\pi H/gT_p^2$

The wave steepness is a fictitious or computation quantity, especially meant to describe the influence of a wave period. This quantity is fictitious as the wave height at the location of the toe is related to the wave length in deep water $(gT_p^2/2\pi)$.

With $\xi_{op} < 2\text{-}2.5$ the waves will tend to break on the seawall slope. This is mostly the case with slopes of 1:3 or milder. For larger values of ξ_{op} the waves do not break on the slope any longer. In that case the slopes are often steeper than 1:3 and/or the waves are

characterized by smaller wave steepness. The general design formula that can be applied for wave run-up on slopes is given by van der Meer and Janssen (1995):

$$R_{u2\%} / H_s = 1.6 \, \gamma_f \, \xi_{op} \quad \text{for } \xi_{op} < 2.0 \qquad \text{(Eqn 2.2a)}$$

$$R_{u2\%} / H_s = 3.0 \, \gamma_f \quad \text{for } \xi_{op} > 2.0 \qquad \text{(Eqn 2.2b)}$$

where, γ_f = reduction factor for slope roughness

For smooth slopes, γ_f = 1.0. For armoured and other slopes, value of γ_f may vary from 1.0 for closed concrete blocks down to γ_f = 0.50 for two layers of open armouring. Different values of γ_f are suggested for different armour types in table 2.1

Table 2.1: Run-up reduction factors for armoured slopes

Type of armour	Reduction factor, γ_f
Smooth concrete/asphalt	1.0
Closed concrete blocks	1.0
Concrete with roughness elements	0.7-0.95
Grass slope	0.9-1.0
1 layer rock armour	0.55-0.6
2 layers rock armour	0.50-0.55
Open concrete armour units	<0.50

Kimura (2000) conducted a two-dimensional hydraulic model test on characteristics of wave run-up at a vertical seawall constructed near the shoreline of Hidaka Subprefecture, Hokaiddo. Characteristics of splash run-up all were surveyed with irregular waves (1 group = 150 waves). The splash run-up height from still water level was read from videotaped image, for statistical operations whose purpose was to generate representative wave data (Rw_{max}, $Rw_{1/10}$, and $Rw_{1/3}$). The experimental wave period ($T_{1/3}$) and offshore wave height (H_o') were varied in the ranges of 2.00 to 3.79 s and 7.0 to 31.0 cm, respectively.

Figure 2.5 shows splash run-up patterns in nine different conditions of three water depths (h) and three offshore wave height (H_o') with a period ($T_{1/3}$) of 2.00 s. At the

same water depth, the higher was the offshore wave height, the higher were the wave energy and the run-up height.
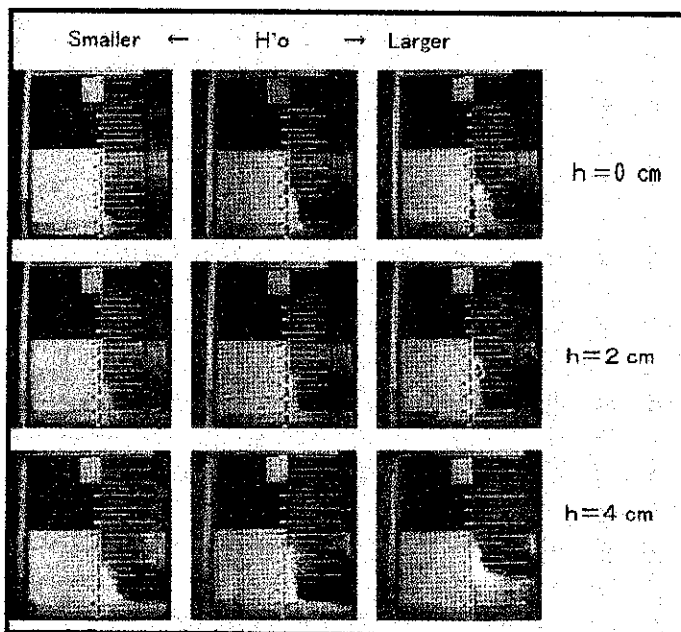
Figure 2.5: Patterns of splash run-up

Figure 2.6 depicts the relationship between the non-dimensional run-up height ($Rw_{1/3}/Ho'$) and the relative depth (h/Ho') using a parameter of Ho'/Lo which is the wave steepness. $Rw_{1/3}/Ho'$ tends to increase with the increase in h/Ho'. As Ho'/Lo decreases, the run-up height increases, which can be attributed to water level rise around the coastline.
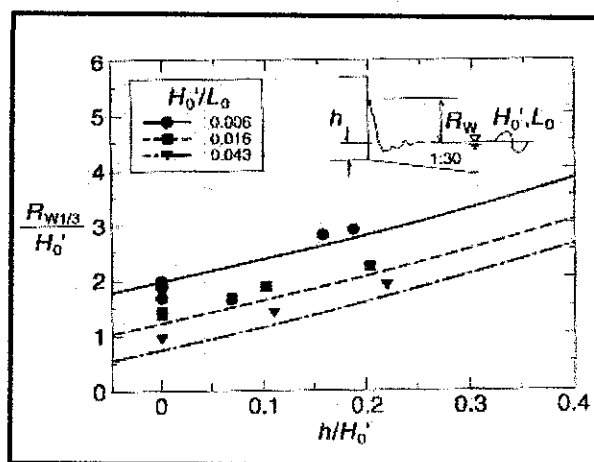
Figure 2.6: Splash run-up heights

Figure 2.7 presents the relationship between representative values of splash run-up height. $Rw_{1/10}/Rw_{1/3}$ is almost constant at 1.3 to 1.8. $Rw_{max}/Rw_{1/3}$ deviates significantly and tends to increase as h/Ho' decreases.
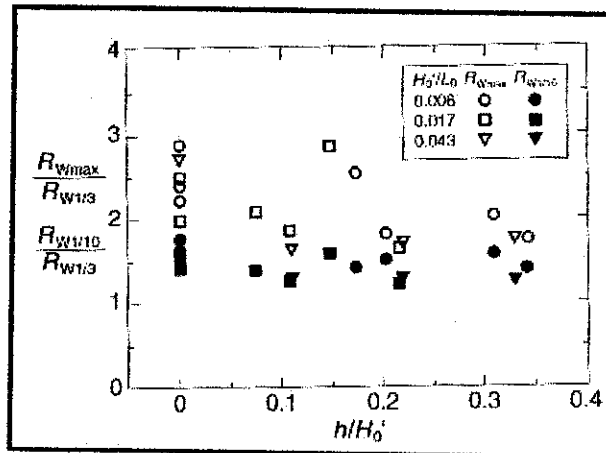
Figure 2.7: Representative values of the splash run - up height

Kimura (2000) also did a model test on splash run-up height reduction for two types of absorbing structures which were wave dissipating blocks and masonry blocks. Figure 2.8 shows the relation between splash run up height with the presence of the absorbing structure $(Rw)_A$, and the relative water depth (h/Ho'). Where $(Rw)_A$ is divided by the value of the vertical seawall under the same conditions, $(Rw)_V$. When h/Ho' equals or exceed 0.3, the splash run-up height can be reduced to nearly half the height of the vertical wall.
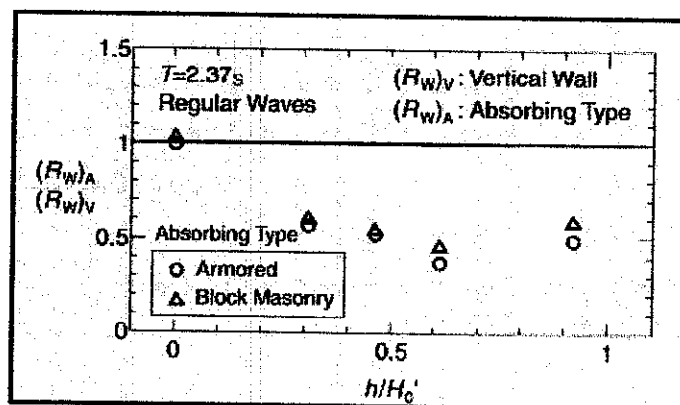
Figure 2.8: Effects of the wave absorbing structures

Base on the results above, the effects of wave absorbing structures to reduce the splash run up height of wave overtopping were clarified.

2.3.2 Wave Overtopping

In the design of seawalls and breakwaters, wave overtopping is the controlling hydraulic response. Wave overtopping will occur if the crest level of a structure is exceeded by the wave run-up. Overtopping is not a continuous process but an intermittent occurrence at times of attack of individual high waves varying from one wave to another. The degree of wave overtopping is normally measured by the mean rate of overtopped water per meter run of the structure ($m^3/s/m$).

Wave overtopping is affected by many factors; even a small modification of the geometry of a structure may change the amount of overtopping. Although there is no reliable conclusion, the increase of wave overtopping by an onshore wind is large when the quantity of overtopping is small and the wind effect decreases gradually as the overtopping rates increases. More accurate estimate of the overtopping rate should be determined through hydraulic model tests.

Allsop (1998) completed a comprehensive analysis of composite vertical structures identifying empirical equations for all three mound types. A parameter, d^*, was identified which determined whether the mound could be classified as large or small. As defined, d^* plays a similar role to the h^* parameter for vertical walls, the difference being that the relative wave height is determined with respect to the water depth over the mound d, rather than the depth at the toe, h. The discharge is then dependent upon whether the mound causes the incident waves to impact on to the structure or to reflect. Overtopping due to impacting waves is significantly greater than that caused by reflecting waves but it is not yet possible to distinguish the parameters that identify the two wave types. In order to take a conservative approach it is therefore recommended that the equations for impacting waves be used. Structures with a small freeboard (R_c/H_{si} < 1.5) were discovered to behave as plain vertical walls. No distinction was made

between deep and shallow water. Figure 2.9 and 2.10 show the parameters for submerged mound and emergent mound.
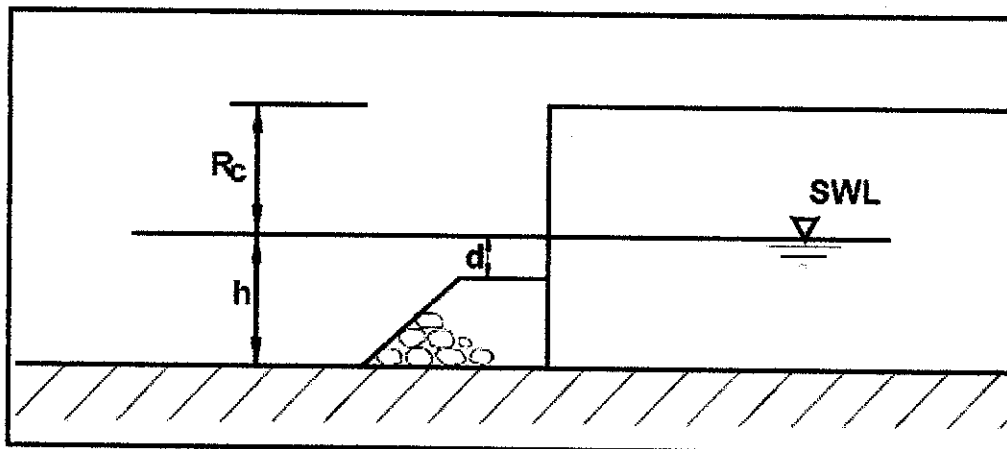
Figure 2.9: Composite vertical wall, submerged mound
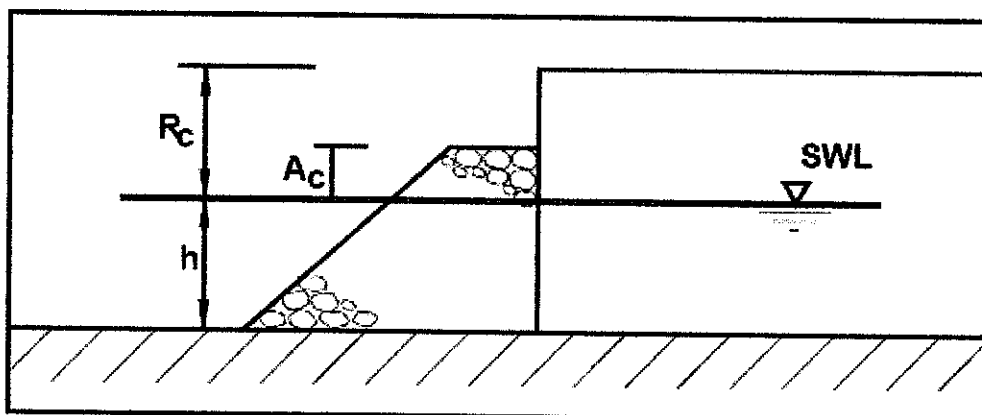
Figure 2.10: Composite vertical wall, emergent mound

The equations discussed are for normal wave attack which will be tested during the laboratory experiment. Determination of d*, is given by the following equation

$$d^* = (d/H_s)(2\pi h/(gT_m^2))$$
(Eqn 2.3)

where, d = the water depth over the mound (m)

   h = the water depth at the toe of the structure (m)

   H_s = the significant wave height at the toe of the structure (m)

   g = acceleration due to gravity (m/s^2)

T_m = the mean wave period at the toe of the structure (s)

When $d* > 0.3$, the mound is classified as small. Overtopping of simple vertical walls, and of composite structures with small mounds, can be predicted using Franco (1994) equation

$$Q\# = 0.03 \exp(-2.5 \, R_c/H_s) \qquad \text{(Eqn 2.4)}$$

where, $Q\#$ = the dimensionless discharge, given by $Q/(gH_s^3)^{0.5}$

Q = the mean overtopping discharge rate per metre run of seawall (m³/s/m)

R_c = the freeboard (the height of the crest of the wall above still water level) (m)

Large mound for which $d* \leq 0.3$, begins to affect the overtopping performance of the seawall. The following equations, which are strictly applicable to impacting waves only, can be employed in order to ensure a conservative design:

$$Q_d = 4.63 \times 10^{-4} \, (R_d)^{-2.79} \qquad \text{(Eqn 2.5)}$$

where, Q_d = the dimensionless discharge given by

$$Q_d = \{Q/(gd^3)^{0.5}\} / d*^2 \qquad \text{(Eqn 2.6)}$$

and, R_d = the dimensionless crest freeboard given by

$$R_d = (R_c/H_s)d* \qquad \text{(Eqn 2.7)}$$

Composite structures with emergent mounds given by Ac > 0 can use Bradbury and Allsop (1988) method with coefficients derived by Madurini and Allsop (1995).

$$Q* = 9.54 \times 10^{-7} \, F*^{-2.24} \qquad \text{(Eqn 2.8)}$$

where, $Q^* = q/(gT_mH_s)$

$$F^* = (R_c/H_s)^2(s_m/2\pi)^{1/2}$$

Wave overtopping can cause inconvenience or danger to personnel and vehicles, interruption to operations and flooding, and can induce instability to the crest and rear amour of the structure. The permissible rate of overtopping water depends on the usage of the crest of the structure or the land behind the structure, the strength of pavement against the impact of falling water mass, and the capacity of drainage facilities. Suggested limits of overtopping are (CIRIA (1991)):

Safety Consideration	Overtopping Rates($m^3/s/m$)
Danger to personnel	3×10^{-5}
Unsafe to vehicle	2×10^{-5}
Damage to unpaved surface	5×10^{-2}
Damage to paved surface	2×10^{-1}

The above values are mean overtopping rates; peak values can be up to 100 times the average.

Kofoed and Burcharth (2000) had verified an existing empirical model for the time variation of overtopping discharge in order to justify the use of model in a parameter range outside the range for which the used equations (eqn 2.9 and eqn 2.10) were originally established. This has been done by comparing experimental data with data simulated by the method used by Jakobsen and Frigaard (1999).

$$P_{ot} = e^{-(IRc/cHs)} \qquad\qquad \text{(Eqn 2.9)}$$

where, P_{ot} = the probability of overtopping

H_s = the significant wave height,

R_c = the crest freeboard and

c = a constant set to 1.21

16

$$P_{V_w} = 1 - e^{-\left(\frac{V_w}{a}\right)^{\frac{3}{4}}} \quad , \quad a = 0.84\frac{qT_m}{P_{ot}} \quad \Leftrightarrow$$

$$V_w = 0.84\frac{qT_m}{P_{ot}}\left(-\ln\left(1 - P_{V_w}\right)\right)^{\frac{4}{3}}$$

<div align="right">(Eqn 2.10)</div>

where, P_{Vw} = the probability of a certain overtopping volume in a wave

V_w = volume of an overtopping wave

q = the mean overtopping discharge and

Tm = the mean wave period.

The comparison of $q_{sim}(t)$ and $q_{meas}(t)$ is done by comparing the results of an analysis done in the following way for each of the discharge time series:

· The discharge time series is divided into N_{window} sub-series each T_{window} long.

· For each of the sub-series the average discharge is calculated so N_{window} average discharge values $q_{window}{}^i$ (for $i = 1 .. N_{window}$) are obtained.

· Each of the values $q_{window}{}^i$ are normalized by the average discharge of the whole time series q ($q_{window}{}^i / q$) and average (which should be 1) and the standard deviation of these values are calculated.

For each of the 2 tests chosen for this analysis, the comparison is made using a window size of 60 s in model scale, corresponding to approximately 60 waves. The results are shown in Figure 2.11.

Furthermore, the analysis have been done using different values for T_{window} for the test with $R = 0.61$. The results are shown in Figure 2.12.
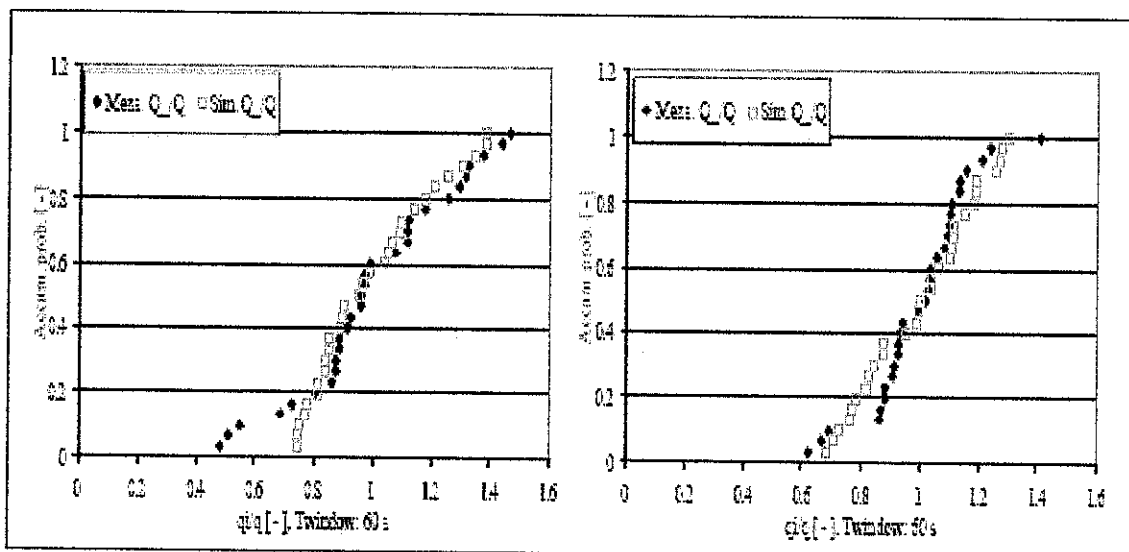
Figure 2.11: Results for the 2 tests with R = 0.61 (left) and 0.37 (right). The accumulated probability density for $q_{window}{}^{i}/q$ is plotted for $q_{sim}(t)$ and $q_{meas}(t)$, respectively.
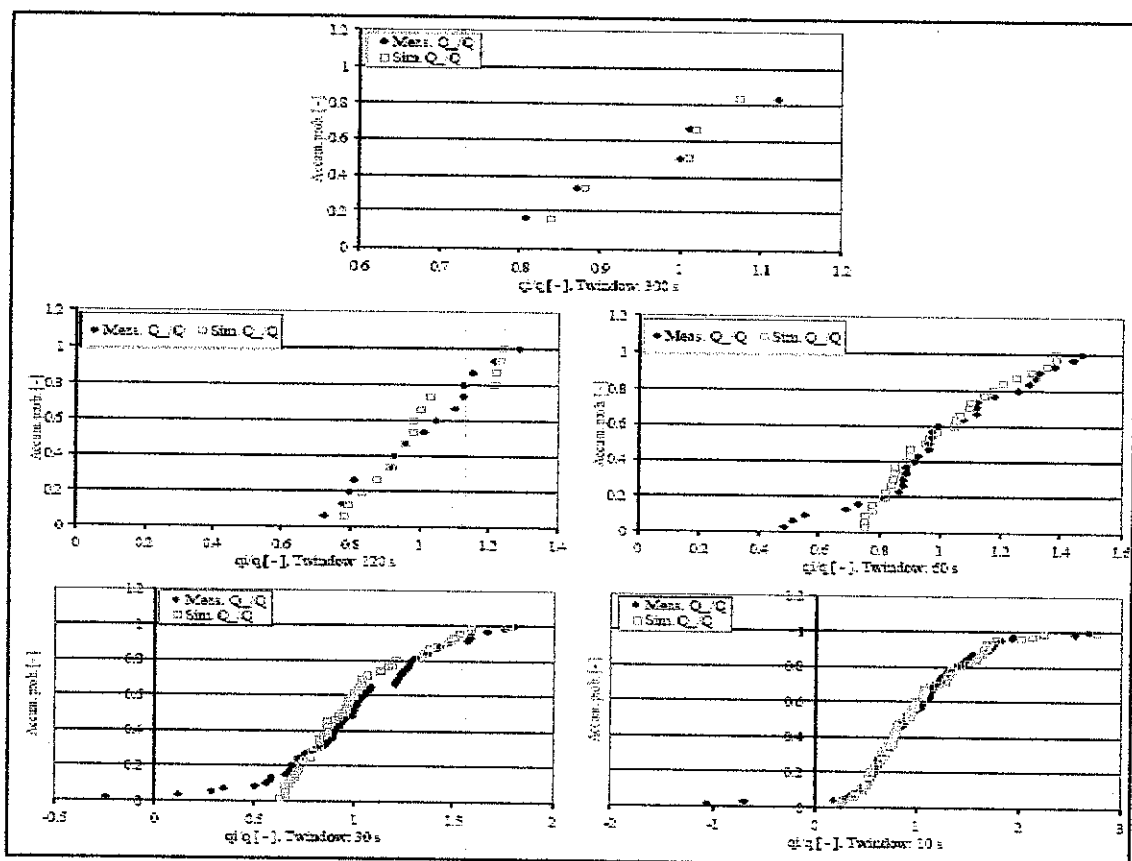
Figure 2.12: Results for test with R = 0.61 where different T_{window} have been applied (T_{window} = 300 s (top), 120 s (middle left), 60 s (middle right), 30 s (bottom left) and 10 s

18

(bottom right), respectively). The accumulated probability density for $q_{window}{}^i/q$ is plotted for $q_{sim}(t)$ and $q_{meas}(t)$, respectively.

This comparison showed a reasonable agreement between the measured and simulated data and it is therefore concluded that the method is applicable also to low values of relative crest freeboards that are typical for ramps used in wave energy converters utilizing the overtopping principle.

By knowing the overtopping rates, Geeraerts (2006) suggested guidance on allowable overtopping discharged and related hazards. Geeraerts distinguished two different approaches to measure and assess wave overtopping. The first approach considers the individual volume per overtopping wave and the second approach considers mean discharge over a certain time interval and per meter run. The main parameters which are considered are significant wave height (H_s) and wave period (T). While the main structural parameters are crest freeboard (R_c), the structure's slope ($tan\alpha$) and the roughness of the structure's slope.

Geeraerts come up with the guidance according to results of frame work of project CLASH done by Allsop (2002). One of the selected fields was composite wall at Samphire Hoe. The first step is based on prototype measurements on wave overtopping and then simulation in small scale laboratory model tests. The hazard occurrence events are presented in Figure 2.13.

Generally, based on the figure, severe events occur during higher wave heights. Apart from that there is no correlation between hazards and tide level. It means hazard occur at both high and low water levels.
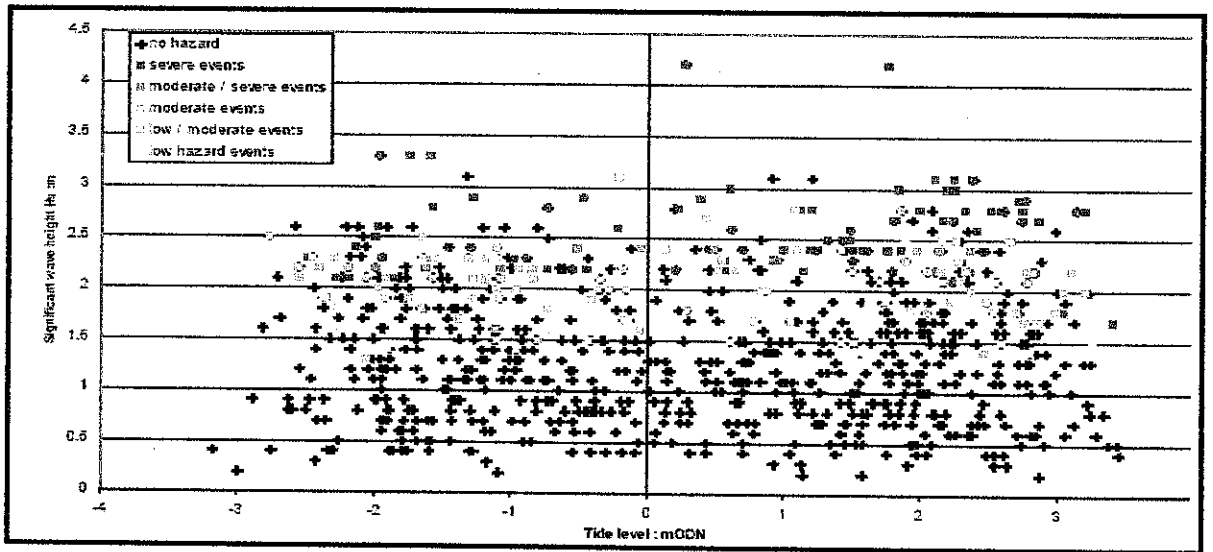
Figure 2.13: Occurrence of hazard at Samphire Hoe

Geeraerts (2006) then defines degrees of overtopping under three levels of severity which are:

- Light overtopping - no impulsive effects or direct structural damage to lightly engineered structures, minor or very local flooding, damage chiefly by inundation only;

- Moderate overtopping - no impulsive effects and little/no direct structural damage to engineered structures, local flooding causing some inundation damage;

- Heavy overtopping - requires significant engineering to resist direct effects without damage, overtopping flows/volumes are unlikely to cause damage to a well engineered defense structure, but local and wider flooding is possible as is flood flow damage to lighter structures.

Figure 2.14: Categorization of overtopping hazards at Samphire Hoe, light, moderate and high.

20

Subsequently limits for overtopping mean discharges or peak volumes are suggested as shown in table 2.2.

Table 2.2: Suggested limits for overtopping mean discharges or peak volumes

Hazard type/reason	Mean discharge, q (l/s per m)	Peak volume, V_{max} (l/m)
Pedestrians		
Unaware pedestrian, no clear view of the sea, relatively easily upset or frightened, narrow walkway or close proximity to edge	0.03	2–5 l/m at high level or velocity
Aware pedestrian, clear view of the sea, not easily upset or frightened, able to tolerate getting wet, wider walkway	0.1	20–50 l/m at high level or velocity
Trained staff, well shod and protected, expecting to get wet, overtopping flows at lower levels only, no falling jet, low danger of fall from walkway	1–10	500 l/m at low level
Vehicles		
Driving at moderate or high speed, impulsive overtopping giving falling or high velocity jets	0.01–0.05	5 l/m at high level or velocity
Driving at low speed, overtopping by pulsating flows at low levels only, no falling jets	10–50	1000 l/m

The permissible overtopping limits guidance is further elaborate in CIRIA (1991) as shown in Figure 2.15.
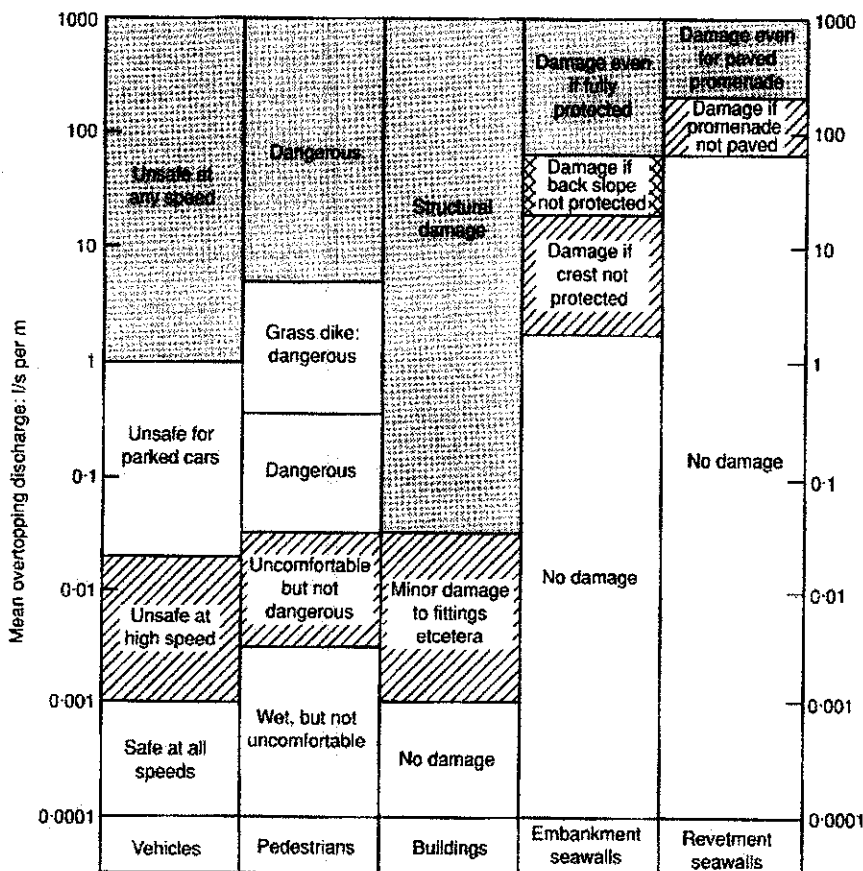
Figure 2.15: Permissible overtopping limits (Owen(1980))

CHAPTER 3

MODEL DESCRIPTION

3.1 INTRODUCTION

In order to investigate the hydraulic performance of composite-type seawalls, physical model tests need to be conducted. The physical model tests will yield quantitative results provided the model is correctly scaled and operated. In this chapter, the structure model will be described in detail. The first part will describe the concrete block of the seawall followed by two composite seawall models.

3.2 CONCRETE BLOCK (MODEL A)

The main unit of a composite seawall is the vertical wall. In this research, the vertical wall was made of a concrete block. It was constructed on a scale of 1:15. Figures 3.1, 3.2 and 3.3 illustrate the concrete block. The dimensions of the concrete block are 29 cm in length (L), 26 cm in height (H), and 10 cm in width (W).
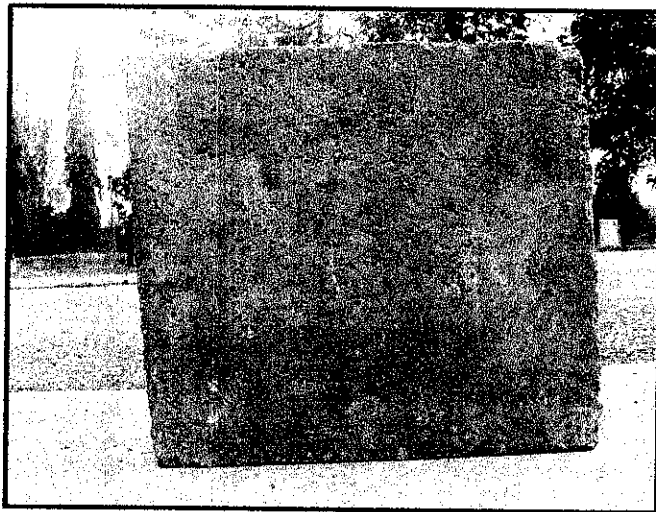
Figure 3.1: Front view of the concrete block
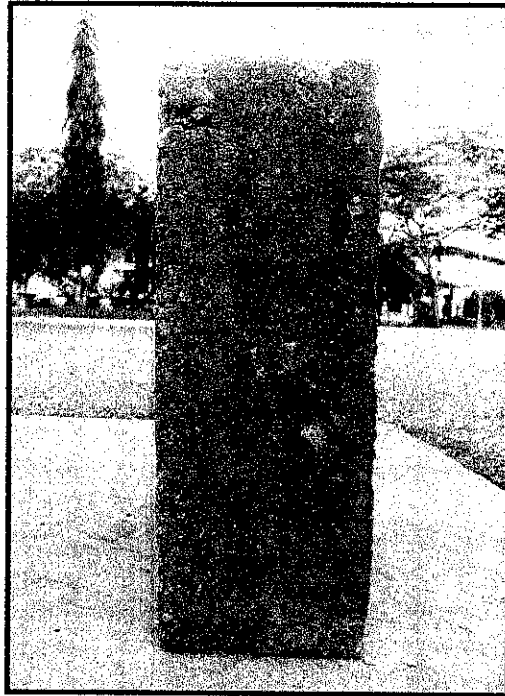
Figure 3.2: Side view of the concrete block
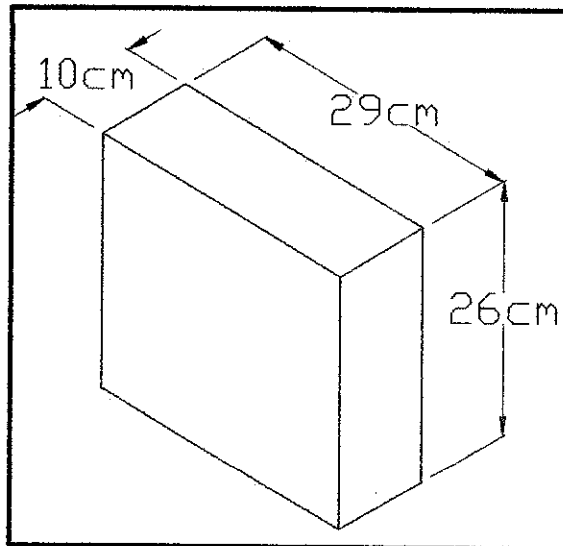
Figure 3.3: Isometric view of concrete block

The concrete block model was fabricated using Ordinary Portland Cement (OPC) and fine aggregates which are sand. Sand occupied 80 percent of the concrete volume which the proportion is 1:5 with one part of OPC to five parts of sand. The diameter of the fine aggregates are varies less than 6mm.

First of all the sand is washed to make sure it is cleaned and free from silt or harmful chemicals. Then the ingredients are mixed to form a mixture of concrete mortar. After the mixture was ready, it was poured into a formwork with desired dimension made of wood. Twenty four hours later, the mixture hardened and it was taken out from the formwork. The concrete block then was soaked in the water for curing purposes.

Besides being the main unit for composite seawalls, the concrete block were tested as vertical seawall. The result obtained was for control purpose and comparison.

3.3 COMPOSITE SEAWALL MODEL WITH QUARRYSTONE AS ARMOUR UNITS (MODEL B)
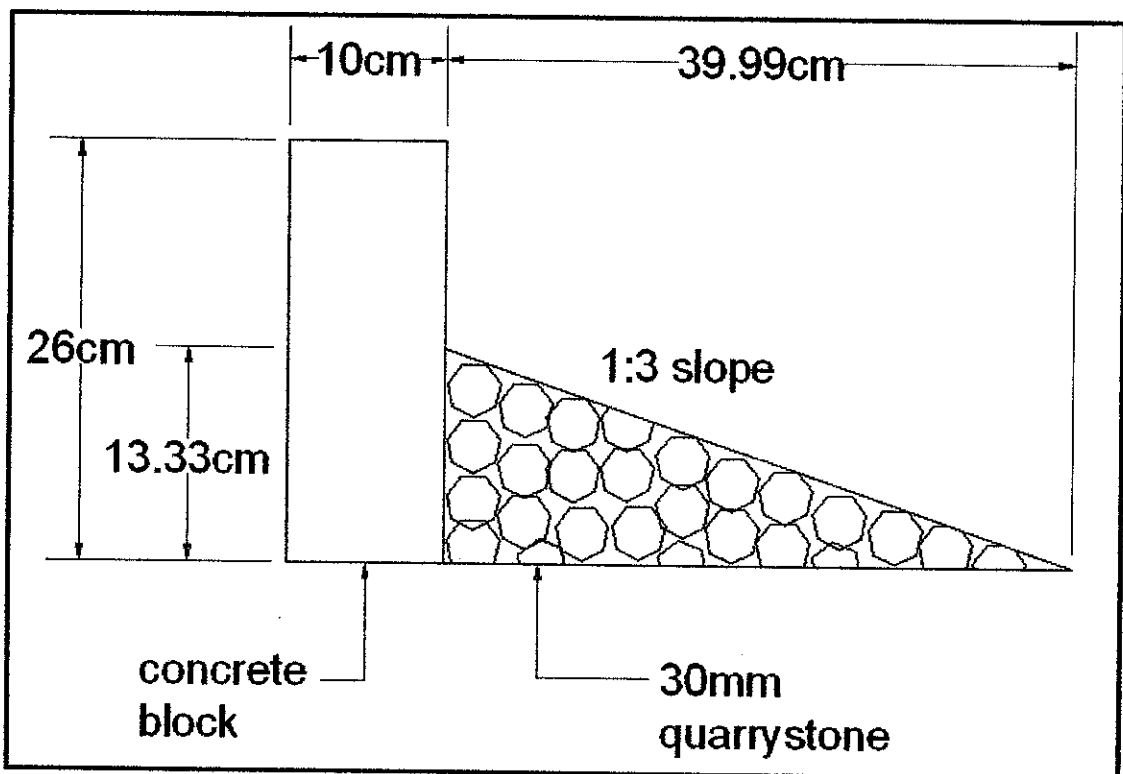
Figure 3.4: Model configuration of composite seawall with quarrystone as the armour units (side view)

Figure 3.4 illustrates the side view configuration of Model B that had been used in this research. The model configuration was constructed with the scale of 1:15 using concrete

24

block as vertical wall and quarrystone as armour units. By using Froude-scaled stability model, the model armor unit specific weight is found as 25.23 kN/m^3 while the weight scale is 3478. Hence, the weight of the model armour unit is 5.64 x 10^{-4} kN. The 30 mm stone size is determined by using equation developed in CIRIA/CUR (1991).

The quarrystone are randomly placed with 13.33 cm in height from bottom of the concrete block with slope of 1:3. Slope of 1:3 is chosen prior to the typical revetment slope in Malaysia.

3.4 COMPOSITE SEAWALL MODEL WITH CONCRETE BLOCKS AS ARMOUR UNITS. (MODEL C)

The armour units of composite seawalls are not restricted only to quarrystone. Various type of armour units exist as an alternative to quarrystone depending on the structure requirements. One of the common armour units applied in Malaysia besides quarrystone is concrete.
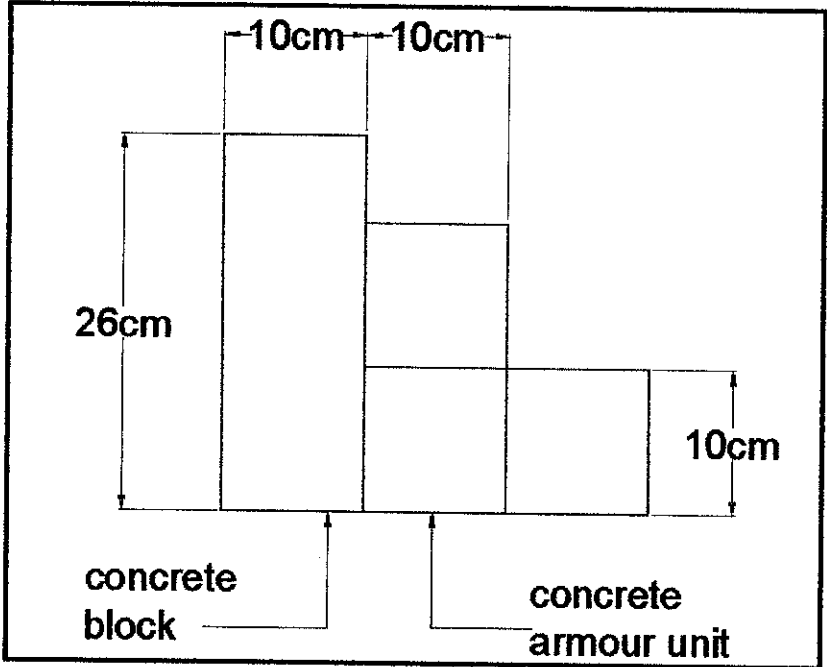
Figure 3.5: Model configuration of composite seawall with concrete block as armour units (side view)

Figure 3.5 shows side view configuration of Model C which uses concrete as armour units. The armour units comprise of several concrete blocks made of the same materials as vertical wall which are OPC and sand. A single concrete unit is 10 cm in height, 10 cm in width and length. The illustration of a single concrete unit is shown in Figure 3.6.
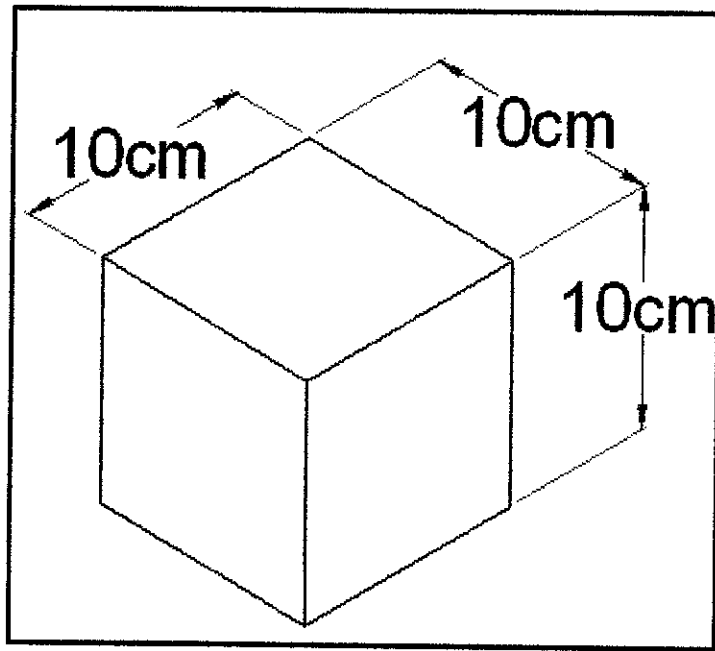
Figure 3.6: Concrete unit

The concrete units were uniformly placed in front of the vertical wall in two layers. The first layer which exactly in front of the vertical wall consists of six concrete units placed in two rows. The second layer which is the toe of the seawall consists of three concrete units placed in one rows. The isometric view of the model is as shown in Figure 3.7.
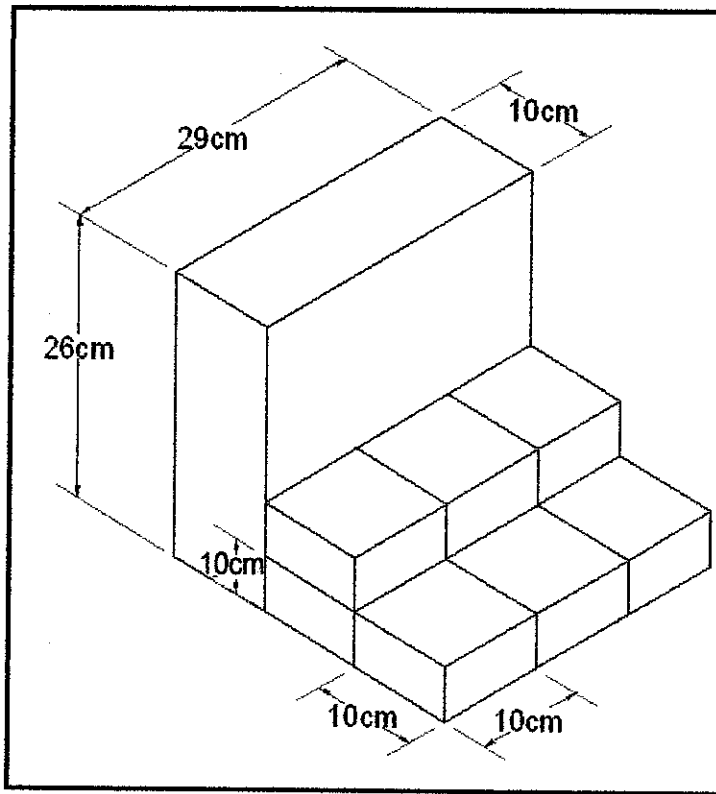
Figure 3.7: Isometric view of composite seawall with concrete as armour units

CHAPTER 4

EXPERIMENTAL SETUP AND PROCEDURE

4.1 INTRODUCTION

This chapter explains the laboratory tools and equipment used in conducting the tests. All tests were carried out in the Coastal and Hydraulics Laboratory, UTP. After the tools are identified, procedures in conducting tests are explained in detail. There were five sets of tests conducted in the research. The tests were preliminary tests where wave periods, T, are measured with respect to different frequencies. Followed by determination of wave incident height, H_i where wave heights are measured with different water depth. Then the determination of overtopping rate for three sets of models which were Model A, B and C.

4.2 LABORATORY TOOLS AND EQUIPMENT

4.2.1 Wave Flume and Flap-Type Wave Generator

The tests are conducted in a 10 m long, 30 cm wide, and 45 cm height wave flume as shown in Figures 4.1 and 4.2. It is commercially named as Modular Flow Channel HM 162. Bed of the wave flume is made of rigid steel and both sides of the wave flume are lined with plexiglass panels for easy observation during the tests.

Figure 4.1: Wave flume

28
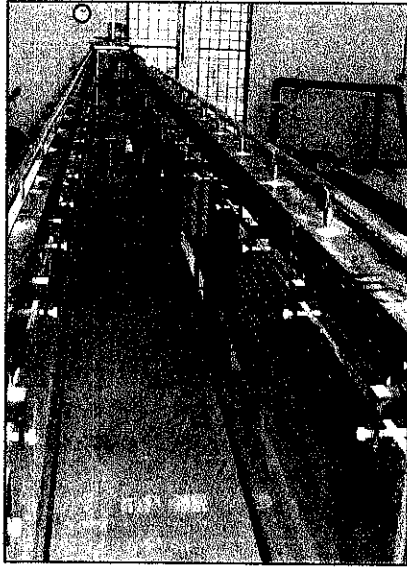
Figure 4.2: Aerial view of wave flume

In the tests, waves are generated by flap-type wave generator which is commercially named as Wave Generator HM 162.41. The components of the wave generator are shown in Figure 4.3. The wave generator is bolted into the surrounding edge of the outlet element of the Modular Flow Channel HM 162 as shown in Figure 4.4. The push rod is connected to the holder of the movable overflow weir. Picture of movable overflow weir is shown in Figure 4.5. The wave generator is driven by a worm gear motor and the rotational speed can be varied by a frequency converter and a potentiometer. The stroke also can be adjusted, causing a change in the wave height. The rotary movement of the motor is converted into a harmonic stroke motion of the movable overflow weir via a crank disk with push rod.

The wave generator operation can be controlled using the switch box as shown in Figure 4.6. The rotational speed gives the stroke frequency of the wave generator and can be adjusted via a 10-gear helical potentiometer. The potentiometer has a scale disk for guaranteeing assignment of the rotational speed. At 100%, the rotation speed is 114 rpm. With a linear characteristic, the rotational speed at 0% is 0 rpm.
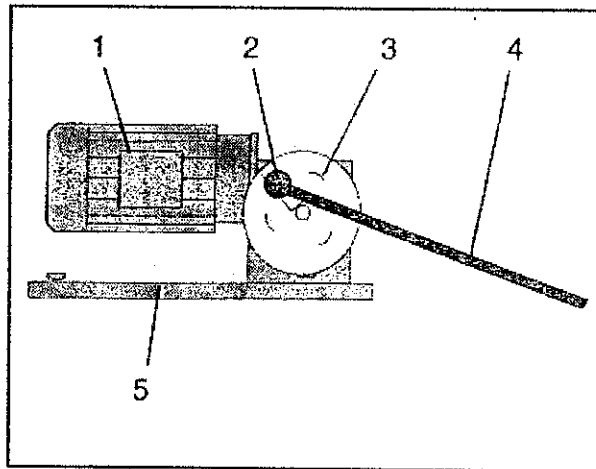
Figure 4.3: Wave generator components. 1. worm gear motor; 2. stroke adjustment; 3.crank disk; 4. push rod; 5. base frame
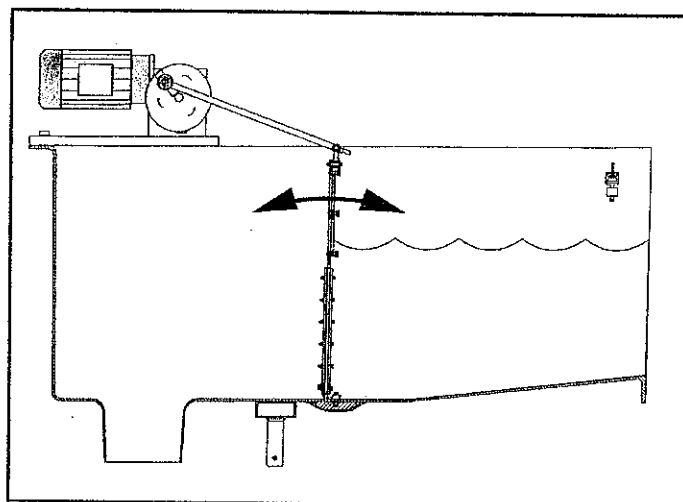
Figure 4.4: Position of wave generator in wave flume

Figure 4.5: Movable overflow weir
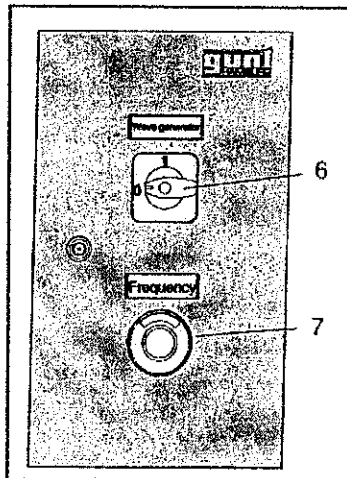
Figure 4.6: Switch box. 6. cam switch ON/OFF; 7. 10 gear helical potentiometer

4.2.2 Instrument Carriage

The unit is designed as a holder for the accessory units which are pitot tube and level gauge. Therefore, the above additional units can be moved to almost any point within the test area of the wave flume. The components of the instrument carriage are shown in Figure 4.7.

31
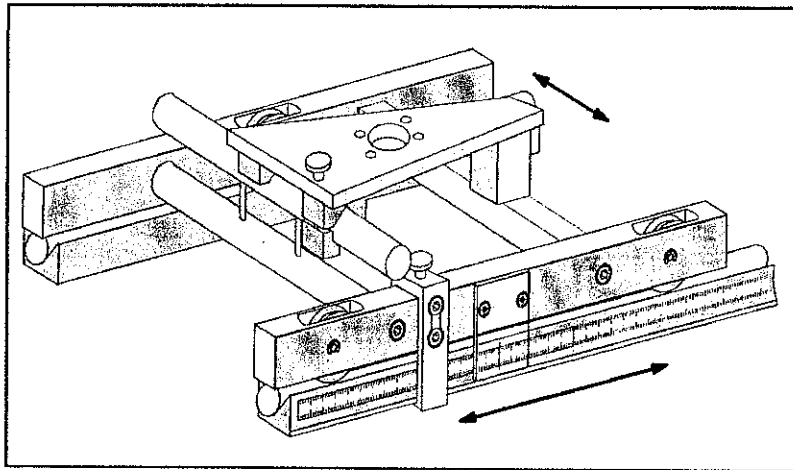
Figure 4.7: Instrument carriage

The instrument holder has smooth - running plastic rollers which lie on the guide rails of the flow channel. This allows the instrument holder to be moved along the entire length of the channel. The unit can be moved on sliding rails transverse to the flow.

The instrument holder can be fixed in any position. A longitudinal and transverse scale with mm markings permits precise positioning of the instrument holder with the additional units.

4.2.3   Hook and Point Gauge

The hook and point gauge is used to measure water levels in the modular flow channel. Combined with the instrument holder, it is possible to carry out measurements over the entire working range of the flow channel since the measuring point can be traced in the longitudinal direction across the width and in the depth of the flow cross section. The components of the hook and point gauge are shown in Figure 4.8.

32

Note:

1. Scanning point;
2. Knurled screw to fix height;
3. Read off point for travel width;
4. Read off point for travel length;
5. Scale for travel length;
6. Knurled screw to fix length;
7. Knurled screw to fix width;
8. Scale for travel height;
9. Read off point for travel height
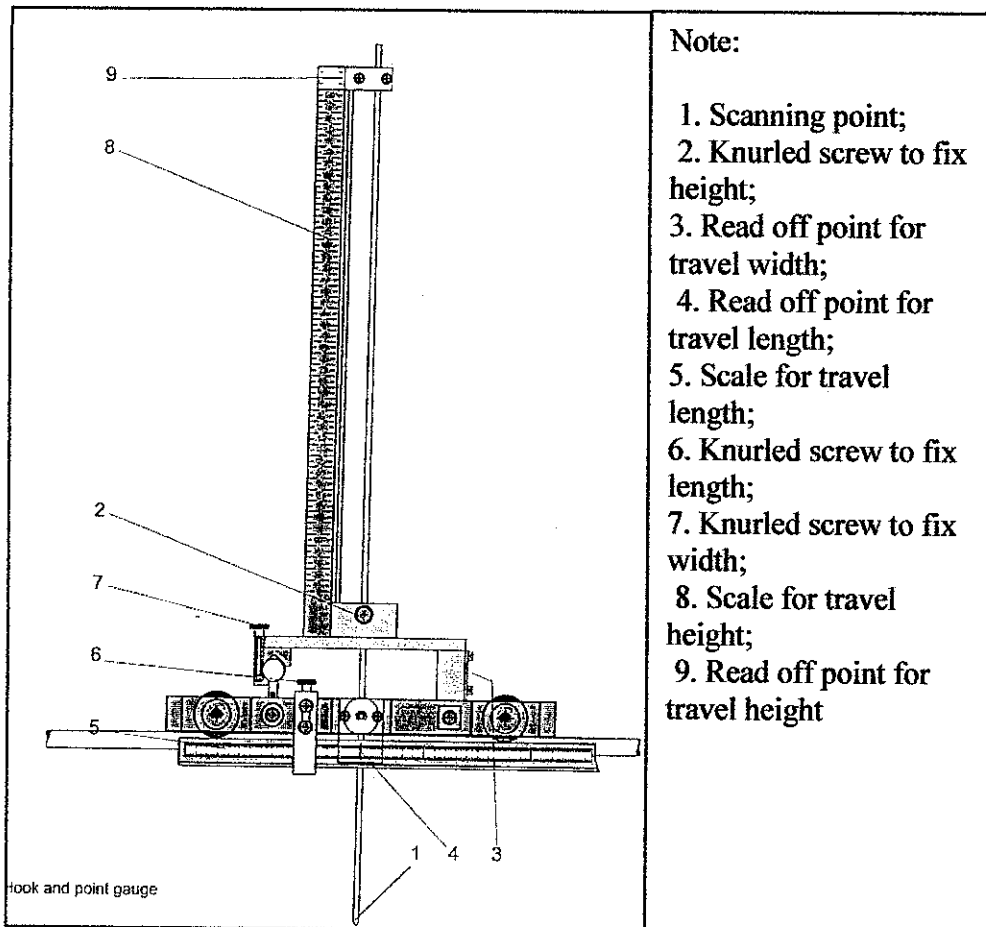
Figure 4.8: Point gauge.

4.2.4 Wave Absorber

The wave absorber is a structure which is located at the reflective boundaries of wave flume to attenuate wave energy through various wave dissipation mechanisms. It consists of wire mesh absorber with adjustable slope angle from 0° to 90° with 120 cm in length, 30 cm in width and 120 cm in slope length. Slope angle of 15° is used during the tests due to its effectiveness in dissipating waves. Figure 4.9 shows the wave absorber.
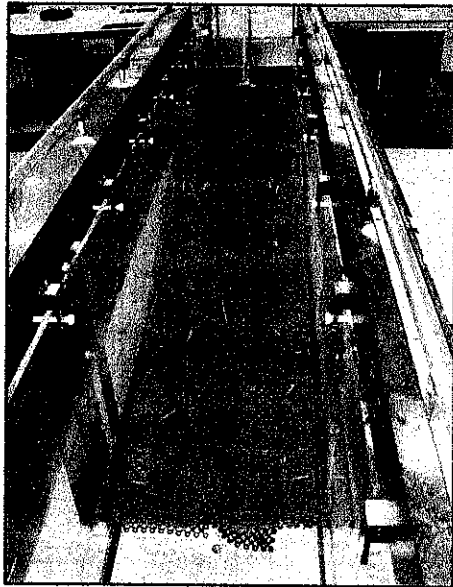
Figure 4.9: Wave absorber

4.2.5 Stop Watch

In the test of measuring the wave period for certain frequency, a digital stop watch is needed to record the time in seconds.

4.2.6 Marker Pen and Scale

A marker pen is needed to mark the crest and trough of waves and a scale is used to measure the wave height.

4.3 EXPERIMENTAL PROCEDURES

This research focused on three major tests which were determination of wave period, T, determination of incident height, H_i, and determination of overtopping discharge, q. Tests procedures are described in the following paragraphs.

4.3.1 Determination of Wave Period, T.

Determination of wave period was mainly for calibration purpose. The wave period, T, was measured with respect to various frequencies. It was determined by obtaining time taken for the crank disk to revolve 10 cycles. The range of frequencies was from 20 to 100 Hz with intervals of 5 Hz. Three readings were taken for each set of frequency in order to get the average wave period. The determination of wave periods was conducted using 200 mm stroke adjustment.

4.3.2 Determination of Incident Wave Height, H_i.

Four series of water depths were tested in determining the incident wave height. The experimental runs were performed in water depths of 18, 20, 22 and 24 cm. The tests were conducted without any model structure located in the flume and the wave heights observed were recorded as incident wave height. The measurements were taken within 15 s after the movable overflow weir started to generate waves. This was to ensure that the wave heights were not expanding due to wave reflection at the end of the flume. It was not advisable to immediately record the wave height after the crank started to revolve because the exact wave height took time to build up. Therefore, the readings were taken within 10 to 15 s after the crank started to revolve. The test is repeated for 13 wave periods with water depth ranging from 0.5 to 2.0 s.

4.3.3 Determination of Overtopping Discharge, q.

The tests were to measure the mean overtopping discharge for Model A, B and C. The composite seawall models setups in the wave flume are as shown in Figure 4.10 and 4.11. The models were equipped with an overtopping tank to collect and measure the volume of overtopped water. Based on the measured volume of overtopped water, the discharge was determined.
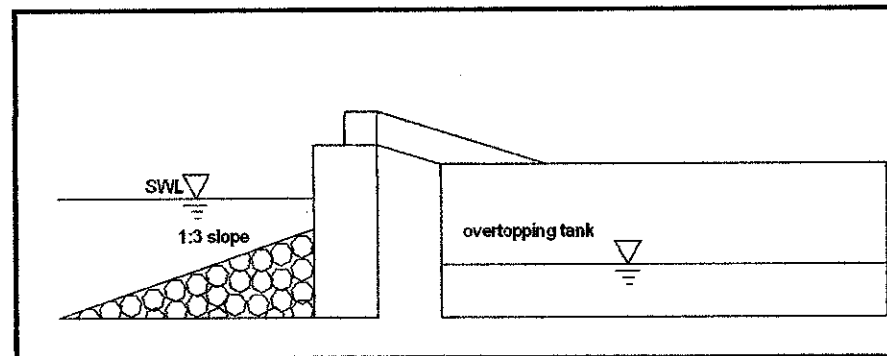
Figure 4.10: Experimental setup for Model B
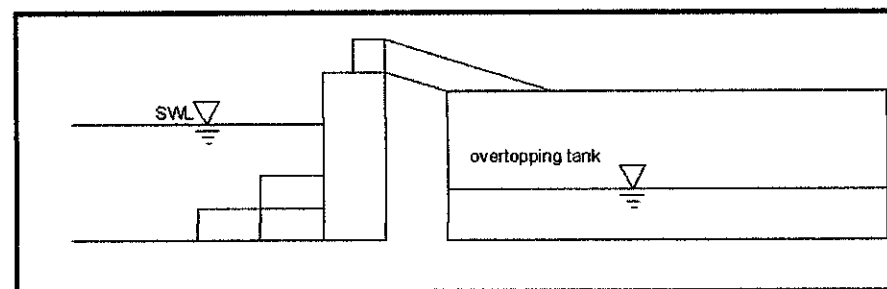
Figure 4.11: Experimental setup for Model C

Each set of tests were conducted in four water depths which were 18, 20, 22 and 24 cm with wave periods ranged from 0.5 to 2.0 s. Then the results were recorded and analyzed. The volume of the overtopped water were measure in milliliters (ml) and the times taken for measured volume of overtopped water to fill were measured in seconds (s). Then the discharge rates were calculated and converted to $m^3s^{-1}m^{-1}$.

36

CHAPTER 5

RESULTS AND DISCUSSION

5.1 INTRODUCTION

The important part of this project is the interpretation of results after tests have been conducted. All the results are presented in tables and graphs and discussed in details. Relationship between wave period, T and frequency, f is first discussed and an equation is developed. Subsequently, relationship between wave period, T and incident wave height, H_i for water depth of 18, 20, 22 and 24 cm is discussed. Equations are also presented for each water depth.

Then the influences of hydraulics parameter to the overtopping rate were discussed. The hydraulics parameters involved were wave steepness and incident wave height. The structural parameters also involved in the analysis which the influence of freeboard crest was discussed.

Finally, the tolerable overtopping discharges for pedestrians, vehicles and buildings were discussed with the guidelines of permissible overtopping discharges developed by Owen (1994).

5.2 DETERMINATION OF WAVE PERIOD, T.

As described in Chapter 4, one complete cycle of the crank disk is recorded in terms of time for few sets of frequencies. Table 5.1 presents the results of wave period values obtained with respect to frequencies ranging from 20 to 100 Hz.

A total number of 17 data sets were taken and transformed into a plot in terms of time, T versus frequency, f. The time used to plot is the average time. The graph is presented in Figure 5.1.

A wave period equation is developed from the plot:

$$T = 280.62 f^{-1.4046}$$

(Eqn 5.1)

Where, T = the time in seconds and,

f = the frequency in Hz.

Table 5.1: Wave period, T, for various frequencies, f

Frequency, f (Hz)	Time, T (s)			
	1	2	3	Average
20	4.50	4.49	4.49	4.50
25	3.13	3.12	3.11	3.12
30	2.38	2.39	2.37	2.38
35	1.92	1.91	1.91	1.91
40	1.61	1.62	1.62	1.62
45	1.38	1.38	1.38	1.38
50	1.00	1.00	1.01	1.01
55	0.91	0.89	0.91	0.90
60	0.83	0.83	0.83	0.83
65	0.76	0.76	0.77	0.76
70	0.70	0.69	0.71	0.70
75	0.65	0.65	0.65	0.65
80	0.61	0.60	0.60	0.60
85	0.55	0.54	0.58	0.56
90	0.52	0.52	0.52	0.52
95	0.50	0.49	0.50	0.49
100	0.49	0.49	0.49	0.49
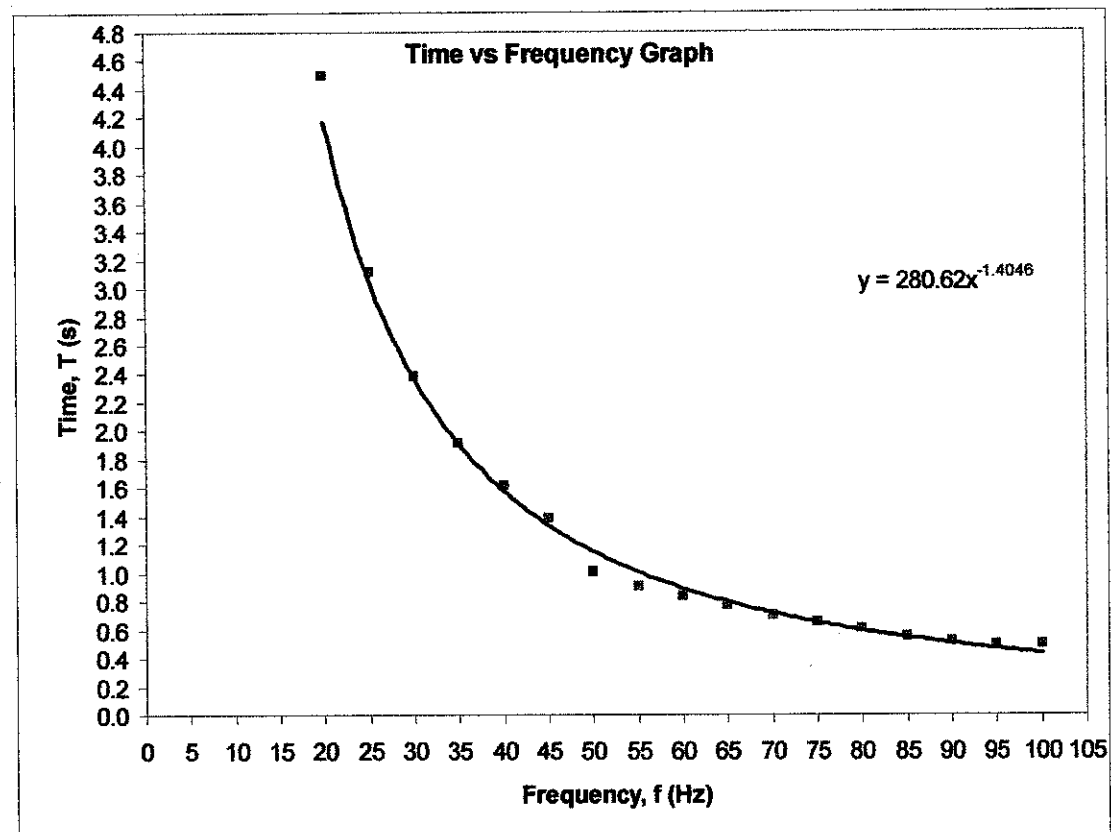
Figure 5.1: Time, T versus frequency, f.

By referring to the graph, it is seem that the wave period, *T* decreases exponentially as frequency, *f* increases. This relationship can be explained as time is inversely proportional to frequency. This curve is then used to determine the accurate frequency for time ranging from 0.5 to 2.0 s.

5.3   DETERMINATION OF INCIDENT WAVE HEIGHT, H_i.

Experimental data of incident wave height, H_i, for water depths of 18, 20, 22 and 24 cm are presented in Tables 5.2, 5.3, 5.4 and 5.5. The results are then plotted in terms of incident wave height, H_i, versus time, *T*. Four sets of curves are plotted in the same plotting area and presented in Figure 5.2.

Table 5.2: Incident wave height, H_i values for water depth of 18 cm

Time, T (s)	Frequency, f (hz)	Water depth, $d = 18$ cm			
		Incident wave height, H_i (cm)			
		1	2	3	Average
0.5	90.62	3.7	3.5	3.7	3.63
0.6	79.59	4.9	4.4	4.2	4.50
0.7	71.32	5.8	5.5	5.3	5.53
0.8	64.85	5.7	5.4	6.6	5.90
0.9	59.64	6.4	6.1	5.7	6.07
1.0	55.33	6.0	6.0	5.2	5.73
1.1	51.70	6.0	5.3	5.8	5.70
1.2	48.59	4.8	5.1	5.0	4.97
1.3	45.90	4.8	4.6	4.6	4.67
1.4	43.54	4.7	4.3	4.1	4.37
1.5	41.45	4.4	4.1	4.4	4.30
1.6	39.59	4.5	4.1	4.2	4.27
1.7	37.92	3.6	4.0	3.6	3.73
1.8	36.41	3.7	3.5	3.2	3.47
1.9	35.03	3.6	3.6	3.4	3.53
2.0	33.78	3.5	3.4	3.8	3.57

Table 5.3: Incident wave height, H_i values for water depth of 20 cm

Time, T (s)	Frequency, f (hz)	Water depth, $d = 20$ cm			
		Incident wave height, H_i (cm)			
		1	2	3	Average
0.5	90.62	3.3	2.8	2.6	2.90
0.6	79.59	4.5	3.9	4.5	4.30
0.7	71.32	5.9	5.5	5.6	5.67
0.8	64.85	6.0	5.4	6.6	6.00
0.9	59.64	6.5	6.4	6.4	6.43
1.0	55.33	5.8	6.6	6.2	6.20
1.1	51.70	6.7	5.8	6.6	6.37
1.2	48.59	5.6	5.5	6.0	5.70
1.3	45.90	5.6	5.5	5.8	5.63
1.4	43.54	5.0	5.3	5.4	5.23
1.5	41.45	4.7	4.4	4.7	4.60
1.6	39.59	4.2	4.0	3.8	4.00
1.7	37.92	3.7	4.2	3.4	3.77
1.8	36.41	3.5	4.6	3.8	3.97
1.9	35.03	3.5	3.7	3.5	3.57
2.0	33.78	3.6	3.4	3.6	3.53

40

Table 5.4: Incident wave height, H_i values for water depth of 22 cm

Time, T (s)	Frequency, f (hz)	Water depth, $d = 22$ cm			
		Incident wave height, H_i (cm)			
		1	2	3	Average
0.5	90.62	3.5	3.6	3.5	3.53
0.6	79.59	4.9	4.8	5.1	4.93
0.7	71.32	6.8	6.7	6.0	6.50
0.8	64.85	7.2	8.2	7.9	7.77
0.9	59.64	8.4	7.6	7.7	7.90
1.0	55.33	8.0	7.8	8.3	8.03
1.1	51.70	7.9	7.8	7.6	7.77
1.2	48.59	7.7	7.8	7.6	7.70
1.3	45.90	6.4	6.9	7.2	6.83
1.4	43.54	5.9	6.2	6.5	6.20
1.5	41.45	5.7	5.1	5.1	5.30
1.6	39.59	5.4	4.5	5.1	5.00
1.7	37.92	5.0	4.5	4.9	4.80
1.8	36.41	5.0	5.4	4.8	5.07
1.9	35.03	4.6	4.7	4.1	4.47
2.0	33.78	4.4	4.7	4.2	4.43

Table 5.5: Incident wave height, H_i values for water depth of 24 cm

Time, T (s)	Frequency, f (hz)	Water depth, $d = 24$ cm			
		Incident wave height, H_i (cm)			
		1	2	3	Average
0.5	90.62	3.8	3.8	4.0	3.87
0.6	79.59	5.5	5.7	4.3	5.17
0.7	71.32	7.5	6.3	6.9	6.90
0.8	64.85	8.2	7.9	7.8	7.97
0.9	59.64	8.4	8.5	8.0	8.30
1.0	55.33	8.0	9.5	8.7	8.73
1.1	51.70	8.6	8.3	8.2	8.37
1.2	48.59	7.5	8.7	7.8	8.00
1.3	45.90	7.8	7.4	7.7	7.63
1.4	43.54	7.2	6.0	6.5	6.57
1.5	41.45	6.9	6.2	6.3	6.47
1.6	39.59	6.3	6.4	6.2	6.30
1.7	37.92	4.9	5.7	5.5	5.37
1.8	36.41	5.7	4.3	5.1	5.03
1.9	35.03	5.1	5.0	4.5	4.87
2.0	33.78	4.3	5.6	4.9	4.93
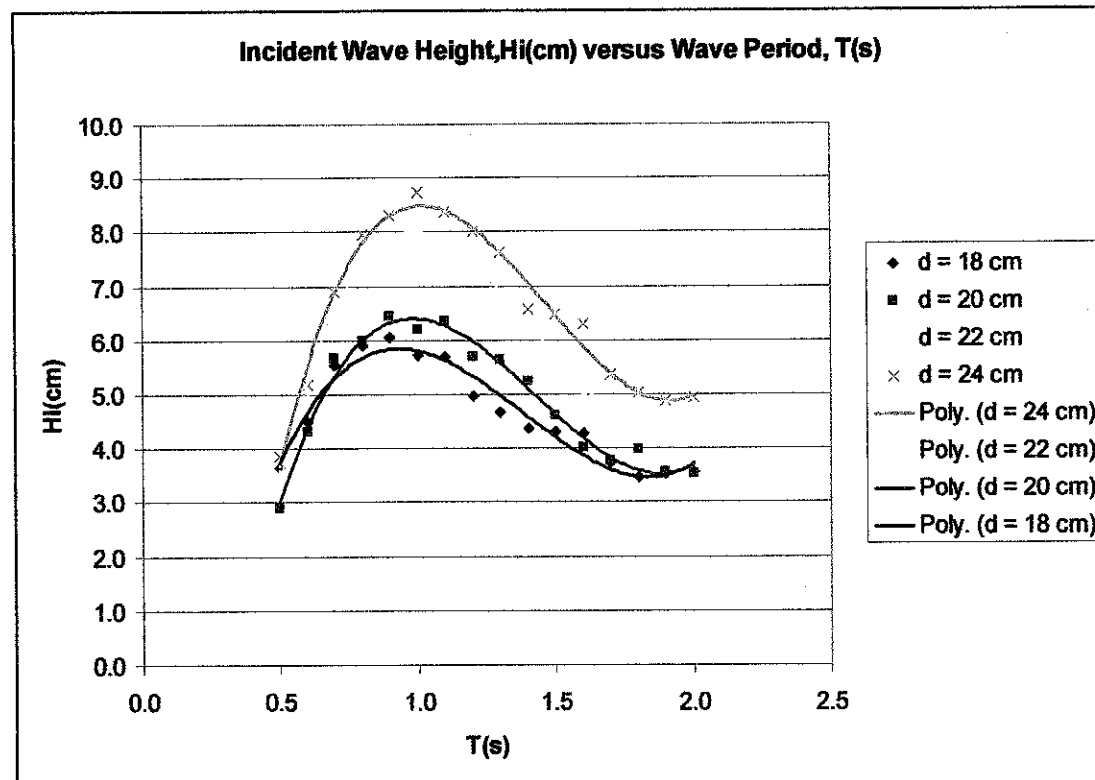
Figure 5.2: Incident wave height, H_i, versus wave period, T.

Incident wave height, H_i, equations for respective water depth, d, are tabulated in Table 5.6 below.

Table 5.6: Incident wave height, H_i equations for respective water depth, d

Water depth, d (cm)	Equation	Equation no.
18	$H_i = 6.4001T^3 - 26.539T^2 + 32.737T - 6.7942$	5.2
20	$H_i = 8.0189 T^3 - 34.395 T^2 + 44.358 T - 11.581$	5.3
22	$H_i = 10.903 T^3 - 46.47 T^2 + 59.821 T - 16.261$	5.4
24	$H_i = 9.8143 T^3 - 43.083 T^2 + 57.043 T - 15.291$	5.5

Referring to the results obtained and the plotted curves, the incident wave height, H_i increased with time, T from 0.5 to 1.1 s for water depth of 18 and 20 cm while the incident wave height, H_i increased with time, T from 0.5 to 1.0 s for water depth of 22 and 24 cm. Then, the incident wave height, H_i started to decrease as the time, T increased beyond 1 s. This proved that the incident wave height, H_i is dependant on wave period, T.

5.4 RELATIONSHIP OF WAVE OVERTOPPING WITH HYDRAULIC PARAMETERS

In this section, the wave overtopping rate obtained during the laboratory sessions were analyzed according to most widely used hydraulics parameters. The purpose was to investigate the influences of the hydraulic parameters to the overtopping rate. The governed hydraulics parameters were wave steepness, H_i/gT^2 and incident wave height, H_i.

5.4.1 Wave Steepness

In this section of analysis, it involved the determination of wave steepness, H_i/gT^2 where H_i is the incident wave height, g is the gravitational acceleration and T is the wave period. The effect of wave steepness on wave overtopping rate of each models are shown in Figure 5.3, 5.4 and 5.5.

5.4.1.1 Model A

The relationship between wave overtopping rate and wave steepness for four different water depths for Model A is shown in Figure 5.3. The data were in the range of $1 \times 10^{-3} < q < 3.5 \times 10^{-3}$ and $1 \times 10^{-3} < H_i/gT^2 < 15 \times 10^{-3}$.

It is found that the value of overtopping rate for water depth of 24 cm is the highest compared to 22, 20 and 18 cm. As the water depth increased, the crest freeboard became limited. Thus, the amount of water overtopped the seawalls increased. This relationship showed that as the water depth increases, the overtopping rate increases accordingly.

Apart from that, overtopping discharge for water depth of 18 cm decreased as the wave steepness increased. Long period waves will have their energy well distributed within the water column. They creates wave set-up in front of the seawall, elevating the water

44

level and limiting the freeboard of the structure. Therefore, the wave overtopping occurrence is more rampant.
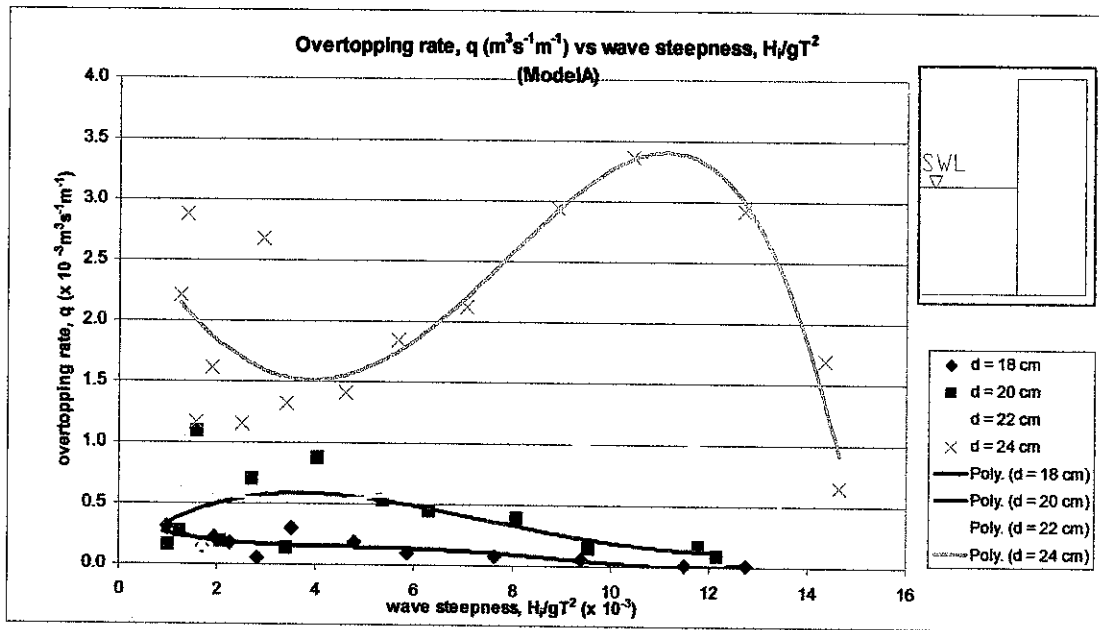
Figure 5.3: Overtopping rate, q ($m^3s^{-1}m^{-1}$) versus wave steepness, H_i/gT^2 (Model A)

It is also observed from the figure that the overtopping rate for water depth of 20, 22 and 24 cm increased to certain wave steepness and then decreased gradually. The increased overtopping rate is due to the increased size of waves acting on a vertical seawall with limited freeboard. Soon after the peaks, it is found that q values reduce significantly. This is because of the fact that when waves are too tall to support themselves, they will break and dissipate their energy into heat and sound. The broken waves/ bores of reduce height are then interact with the vertical wall and cause some wave overtopping.

5.4.1.2 Model B

The effect of wave steepness on overtopping rate for Model B can be seen in Figure 5.4. For a given water depth, the overtopping rate increased to certain range of wave steepness and then decreased. This is due to the effect of increased in wave incident height and increased time period. It is found that the plotting patterns of the graphs representing different water depths are agreeable to those shown in Figure 5.3.

45

As can be seen in Figure 5.4, the overtopping rates for $d = 18$ cm are somewhat limited as compared to those of greater water depths. Wave breaking above the slope was due to limited depth of water. It reduces of momentum of the wave in advance. Furthermore, the water particles orbits were greatly affected by the quarrystone inclined slope fronting the vertical seawall.
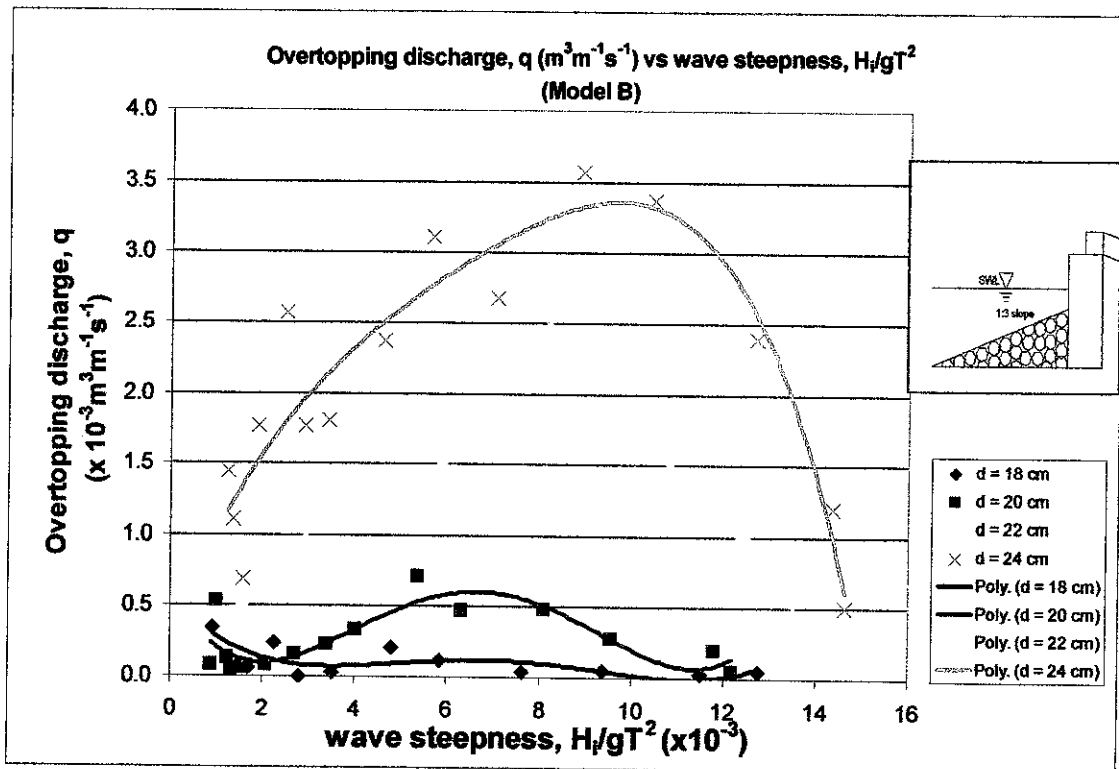
Figure 5.4: Overtopping rate, q ($m^3s^{-1}m^{-1}$) versus wave steepness, H_i/gT^2 (Model B)

For $d = 20$, 22 and 24 cm, it is observed that the waves break when $H_i/gT^2 = 10 \times 10^{-3}$. The overtopping rates increased gradually as H_i/gT^2 increased from 0 to 10×10^{-3}. The increased values were affected by increased H_i for each water depth. The figure also shows that as the wave heights and overtopping rates increased rapidly as the water depths increased.

After the waves break, the overtopping rates decreased as H_i/gT^2 increased. It is expected because when the waves break, the wave heights became smaller. As a result, smaller values of overtopping rates are obtained.

46

5.4.1.3 Model C

Figure 5.5 shows the relationship of overtopping discharge with wave steepness for Model C. The values of overtopping discharge for $d = 24$ cm were relatively high very and scattered compared to d = 22, 20 and 18 cm. It can be seen that overtopping rate for $d = 18$ cm were in the range of $1 \times 10^{-4} < q < 0.1 \times 10^{-3}$ and $1 \times 10^{-4} < q < 1 \times 10^{-3}$ for $d = 20$ and 22 cm. The wave overtopping rates were somewhat small for $d = 18, 20, 22$ cm because the waves broke and splashed when it reached the stacked concrete cubes before overtopped the seawalls. Smaller water depth gave smaller overtopping rate. Hence, the amount of overtopping was reduced. It shows that the overtopping rates are less dependent upon H_i/gT^2 for d = 18, 20 and 22 cm. As for d = 24 cm, the surface water level was 2 cm below the crest of the seawall. Thus, the tendency of large overtopping volume was high. However from the figure, the overtopping rates become unpredictable and scattered when $d = 24$ cm. Therefore no definite conclusion can be made based on the experimental results.
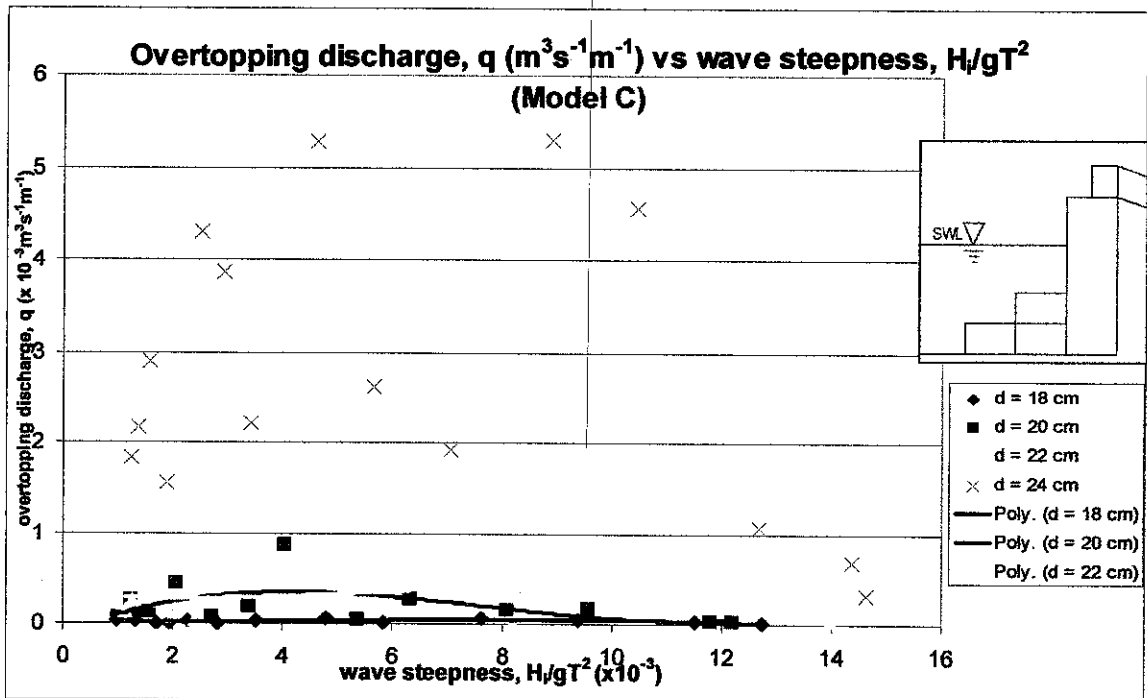
Figure 5.5: Overtopping rate, q ($m^3 s^{-1} m^{-1}$) versus wave steepness, H_i/gT^2 (Model C)

47

Based on the observation, the values of overtopping rates for Model C are relatively small as compared to those of Model A and Model B, except in the water depths of 24 cm. This shows that stacked concrete cubes are effective in smaller water depth. Apart from that, it can prevent scour problem as well as trigger wave breaking on the concrete cube. It is also easy to install and maintain.

5.4.2 Incident Wave Height

In this section, the influences of incident wave height to overtopping rate were investigated. The graphs and discussion of each model were stated in the following section.

5.4.2.1 Model A

A plot to show the relationship of overtopping rate and incident wave height for Model A is shown in Figure 5.6.
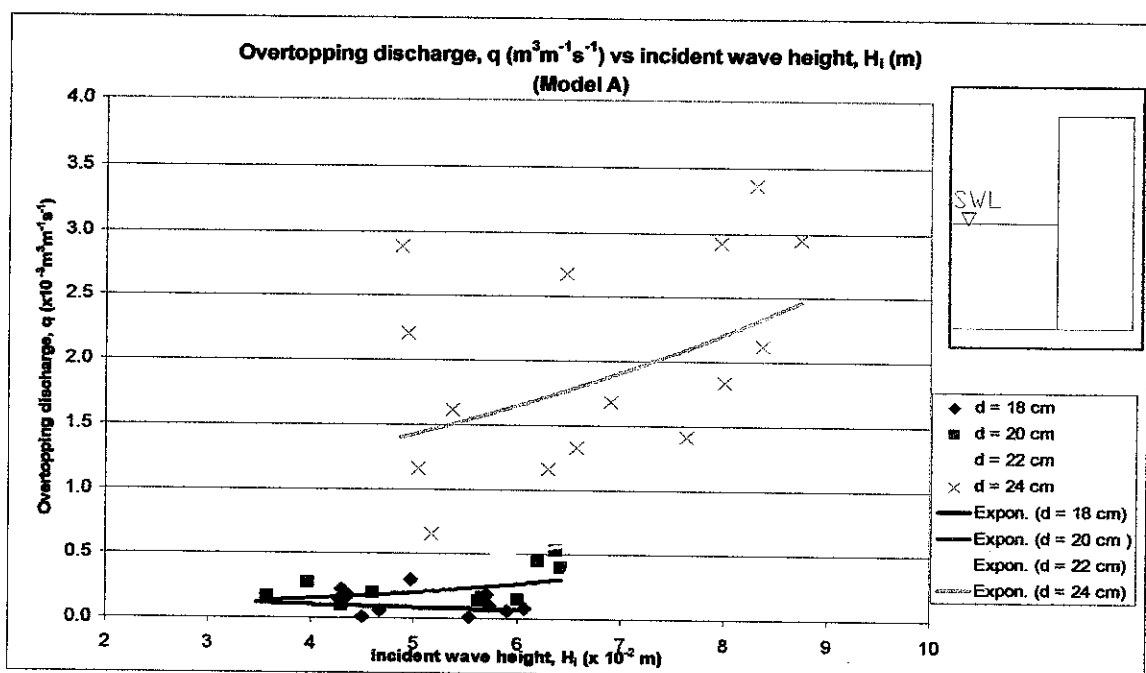
Figure 5.6: Overtopping rate, q $(m^3 s^{-1} m^{-1})$ versus incident wave height, H_i (m) (Model A)

It is observed from the figure that the amount of overtopping rate increased as the incident wave height increased with an exponential correlation even though the data was scattered.

For $d = 18$ cm, a constant overtopping rate with respect to a range of incident wave height was obtained. It is expected that an overtopping discharge of 0.3 x 10^{-3} $m^3m^{-1}s^{-1}$ is obtained when 4 cm < H_i < 6 cm. It is anticipated that as H_i > 6 cm, the overtopping values will increase gradually.

As for $d = 20$ and 22 cm, the overtopping rates increased slowly as a respond to increased incident wave height. While for $d = 24$ cm, the overtopping rates increased drastically when the incident wave height increased.

From the results, it shows that deep water with high waves produce high amount of overtopping volume. This could cause inundation of the hinterland, flooding of the coastal areas and damages to structures.

5.4.2.2 Model B

The relation between overtopping rate and incident wave height for Model B is given in Figure 5.7. Overall, the experimental results show the overtopping rate increased with the increment of incident wave height. For $d = 18$ cm, the waves overtopping were insignificant. This is again due to the limited water depth and substantial crest freeboard, limiting the rough waves from reaching the crest of the structure.

It is clearly shown that for $d = 20$, 22 and 24 cm, the overtopping rate increased with wave height in an exponential manner. The data of overtopping rate for Model B were less scattered as compared to Model A. The range of overtopping rate was 1×10^{-3} < q < 3.6×10^{-3}. This indicated that the sloped quarrystones used for wave dissipation did not help in reducing the overtopping rate. The sloping quarrystone helped the waves to run up to the vertical wall instead of dissipate waves. When the slope was submerged with

water depth of 22 or 24 cm, the effect of having the sloped quarrystone was not significant and the waves action were the same as wave action on vertical wall.
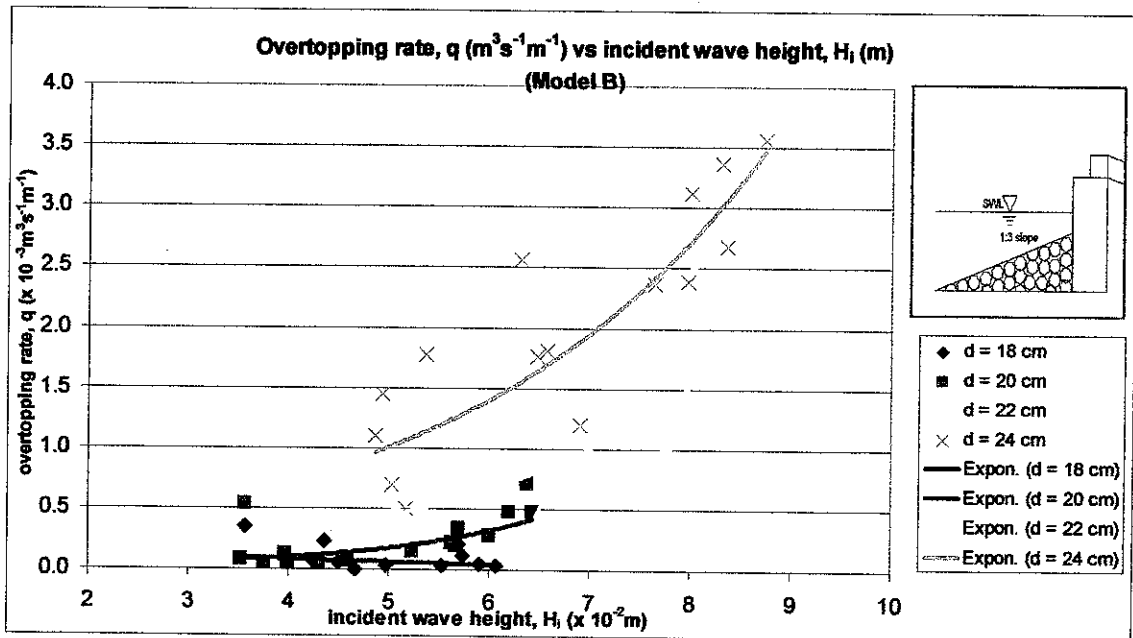
Figure 5.7: Overtopping rate, q ($m^3s^{-1}m^{-1}$) versus incident wave height, H_i (m) (Model B)

5.4.2.3 Model C

Relationship between overtopping rate and incident wave height for Model C is provided in Figure 5.8.

It is observed that the data points for q in a depth of 24 cm are very scattered. Nevertheless, most of the data values generally increase with the increase of H_i. The scattered data may be due to the effect of violent wave overtopping. The waves generated were rapid and a lot of splashing observed during the experiment. These may contribute to variation in overtopping volume data.
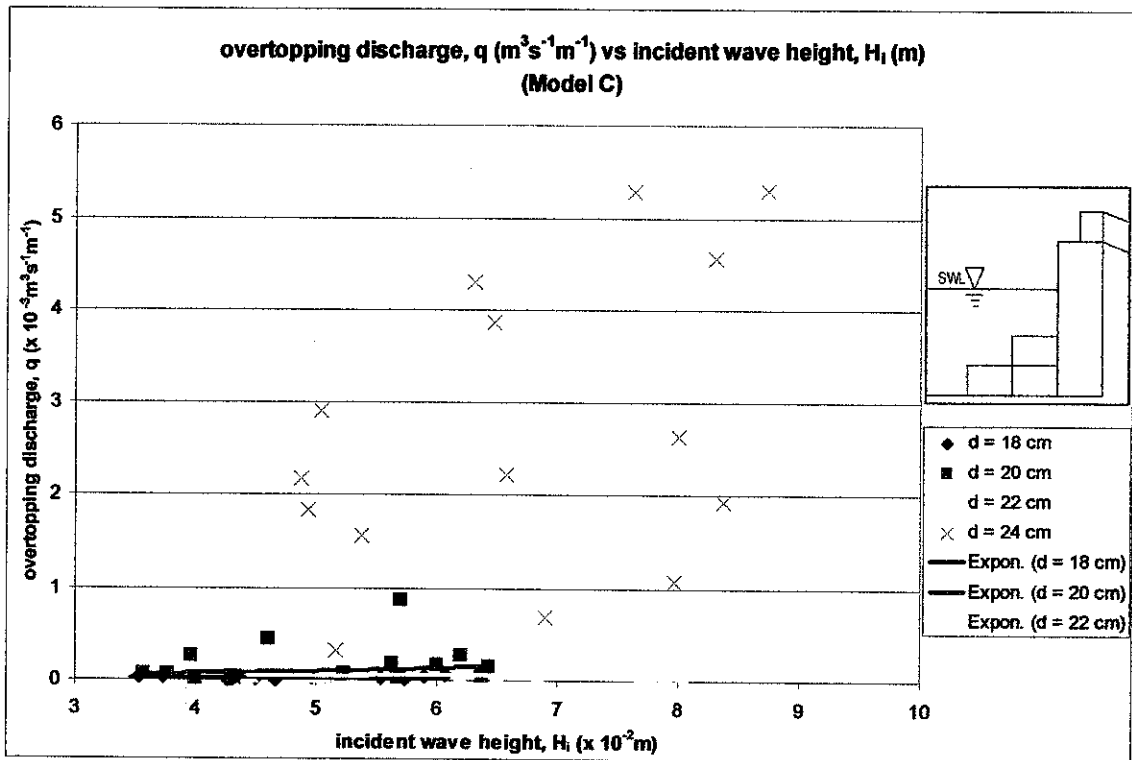
Figure 5.8: Overtopping rate, q ($m^3s^{-1}m^{-1}$) versus incident wave height, H_i (m) (Model C)

It can also be seen that the plots showing the overtopping rate for $d = 18$, 20 and 22 cm are closely related to each other. Most of the data points range from 1×10^{-4} $m^3s^{-1}m^{-1}$ to 1×10^{-3} $m^3s^{-1}m^{-1}$.

From the analysis of influence of incident wave height to overtopping rate for all models, it can be said that the incident wave height has a major influence to wave overtopping. The findings are agreeable to Shankar and Jayaratne (2003), in which the wave overtopping increases almost exponentially with the wave height. The results are also confirmed by the results yielded by Juhl and Sloth (1994) who found that the overtopping rate increased as the water depth increased.

5.5 TOLERABLE WAVE OVERTOPPING RATE

In this section, the effects of wave overtopping rates were estimated using the suggested limits for safety by Owen (1980) (Figure 2.15). The overtopping rates were expressed as flow rate per meter run of seawall, which was l/s per m. Risk assessment were carried out to study the effect of wave overtopping on the following aspects:

i)   Pedestrians

ii) Vehicles

iii) Buildings

iv) Embankment seawalls

The values overtopping rates for each model were scaled up by 15 times in order to get the corresponding discharge of prototype. The calculations are as follows:

i)   The velocity ratio between the prototype and the model is

$$V_p/V_m = (L_p/T)/(L_m/T) = (L_p/L_m) = L_r = 15$$

ii) The area ration between the prototype and the model is

$$A_p/A_m = L_p^2/L_m^2 = L_r^2 = 15^2 = 225$$

iii) The discharge ratio is

$$Q_p/Q_m = (A_pV_p)/(A_mV_m) = (225)(15) = 3375$$

iv) Thus, the corresponding discharge in the prototype is

$$Q_p = 3375(Q_m)$$

v)   The prototype discharge per meter is

$$Q_m per\ m = Q_m/(3375 \times 0.29)$$

where 0.29 is the length of the tested model in meter

5.5.1 Pedestrians

The tolerable wave overtopping rates for pedestrians for Model A, B and C are shown in Figure 5.9, 5.10 and 5.11.
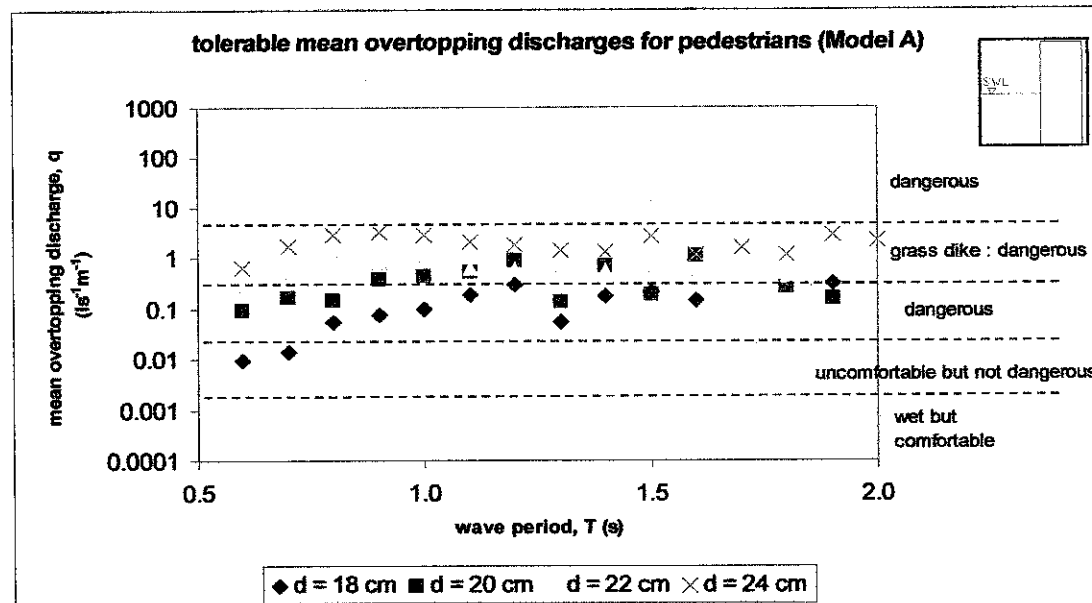
Figure 5.9: Tolerable overtopping rates for pedestrians (Model A)

In estimating the effects of experimental overtopping rates to pedestrians, graphs of overtopping rates versus time period were plotted. There were basically three zones of limits for pedestrians namely wet but comfortable, uncomfortable but not dangerous to the pedestrians and dangerous to pedestrians. From Figure 5.9, it can be seen that the observed overtopping rates were in the range of 0.01 to 5 $ls^{-1}m^{-1}$. The risk level with respect to different water depths for 0.5 s < T < 2.0 s can be presented in Table 5.7.

From the table, the risk level for d = 18 and 20 cm is dangerous while d = 22 and 24 cm is grass dike: dangerous. The implications of the risk level are the pedestrians could not have a clear view of the sea and might fall from the walkway. The pedestrians also might get hurt due to the wave overtopping.

53

Table 5.7: Risk level for pedestrians (Model A)

Water depth, d (cm)	Risk level
18	dangerous
20	dangerous
22	Grass dike : dangerous
24	Grass dike : dangerous

As for Model B (Figure 5.10), the overtopping rates were in the range of 0.006 to 5 ls⁻¹m⁻¹.
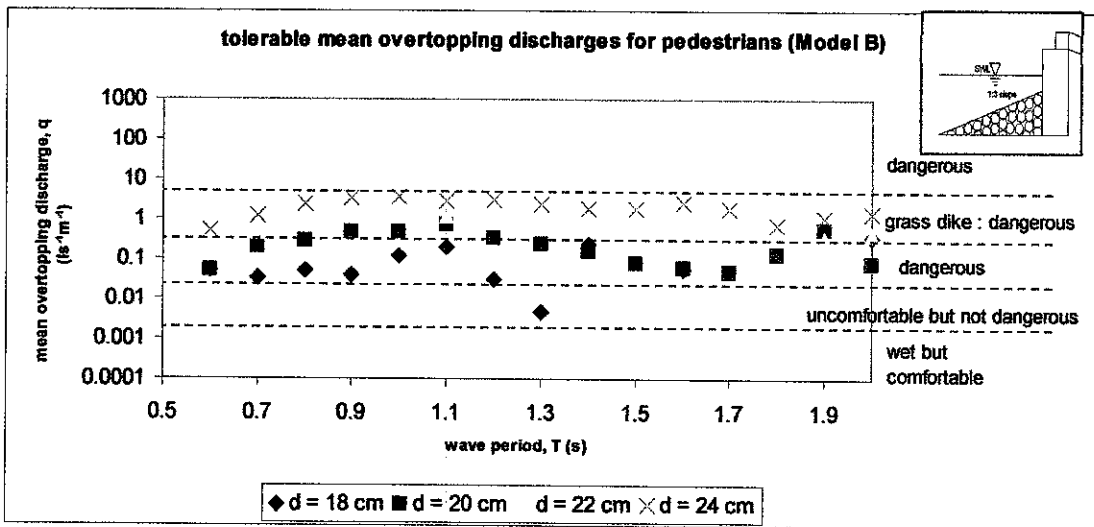
Figure 5.10: Tolerable overtopping rates for pedestrians (Model B)

The overtopping rates for each water depth fell into dangerous zone accept for one overtopping rate of d = 18 cm with time period of 1.3 s, fell into uncomfortable but not dangerous zone. Table 5.8 represented the summarize risk level for Model B.

Table 5.8: Risk level for pedestrians (Model B)

Water depth, d (cm)	Risk level
18	dangerous
20	dangerous
22	Grass dike : dangerous
24	Grass dike : dangerous

The risk level for pedestrians for Model B is agreeable to risk level for pedestrians for Model A (Table 5.7). Thus the implication will be the same where the pedestrians will fall from the walkway, having the possibilities to get hurt and could not have a clear view of the sea.

Figure 5.11 shows the tolerable overtopping rate for Model C with the range of 0.008 ls^{-1}m^{-1} < q < 7 ls^{-1}m^{-1}. For d = 18 cm, there was an overtopping rate with wave period of 1.5 s fell in wet but comfortable zone. The overtopping rates with wave period of 1.3 and 1.6 s fell into uncomfortable but not dangerous zone and the remaining overtopping rates were in the dangerous zone. For d = 20 cm, the overtopping rate during the time period of 0.7 s was in between uncomfortable but not dangerous zone and dangerous zone. The remaining overtopping rates of d = 20 cm were in the dangerous zone together with the overtopping rates for d = 22 and 24 cm. The summarize risk level is shown in Table 5.9.

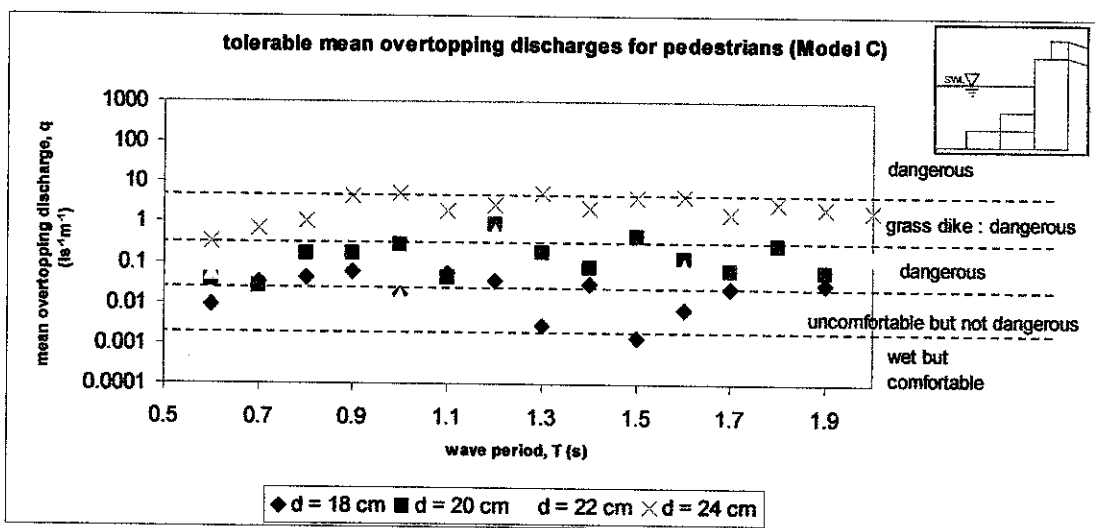*Figure 5.11: Tolerable overtopping rates for pedestrians (Model C)*

For d = 18 cm, the overtopping rates fall into uncomfortable but not dangerous level. The pedestrians will get wet but not going to fall from the walkway. Pedestrians also could have a clear view of the sea. For d = 20, 22 and 24 cm, the implications would be the same as implications for Model A and Model B.

Table 5.9: Risk level for pedestrians (Model C)

Water depth, d (cm)	Risk level
18	Uncomfortable but not dangerous
20	dangerous
22	dangerous
24	Grass dike : dangerous

Despite having most of the overtopping rates in the dangerous zone, the ranges of data for Model C were small compared to Model A and B. Taken $d = 22$ cm data for each model as example, the range of overtopping rates for Model A, B and C were from 0.2 to 1 $ls^{-1}m^{-1}$, 0.1 to 3 $ls^{-1}m^{-1}$ and 0.01 to 0.7 $ls^{-1}m^{-1}$ respectively (Figure 5.12). This was due to the concrete cubes placed in front of the vertical wall in stepped arrangement. The stepped concrete cubes helped in reducing the overtopping by having the waves splashed and broke to its vertical surfaces before reaching the vertical wall.
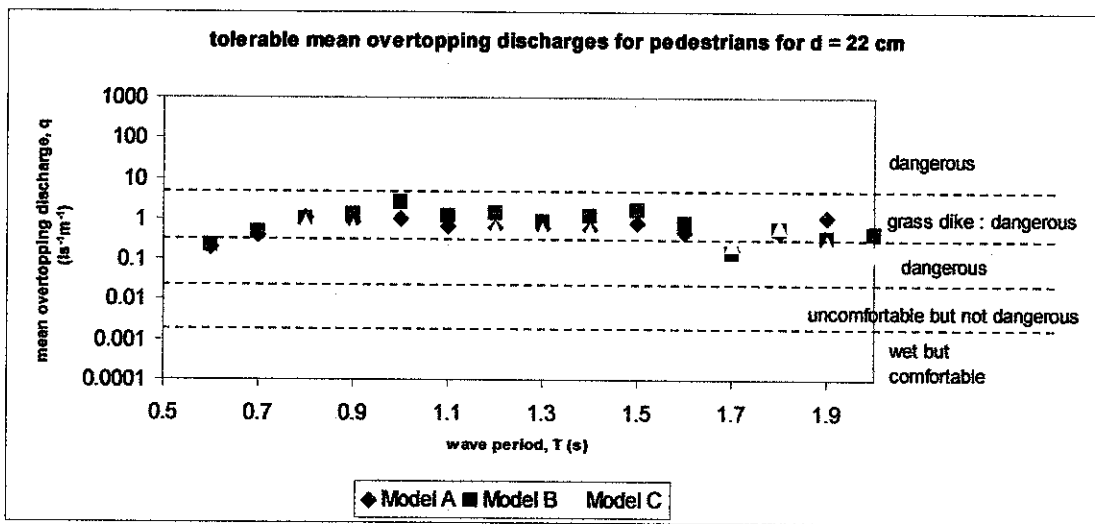

Figure 5.12: Tolerable overtopping rates for pedestrians (d = 22 cm)

Besides considering the effect of overtopping rates to pedestrians, consideration on vehicles also was taken into account. The discussion on limits for vehicles was in the next section.

5.5.2 Vehicles

Overtopping limits for vehicles were divided into four zones i.e. safe at all speeds; unsafe at high speeds; unsafe for parked cars and unsafe at any speed. The chart of tolerable overtopping discharges for vehicles for Model A is shown in Figure 5.13.

For $d = 18$ cm, the overtopping rates fell into two zones which were unsafe at high speeds and unsafe for parked cars. The overtopping rates during time period of 0.6 and 0.7 s were in the unsafe at high speeds zone. All overtopping rates for $d = 20$ and 22 cm were in the unsafe for parked cars zone while for $d = 24$ cm, the overtopping rates were in unsafe at any speeds zone except for overtopping rate during time period of 0.6 s.

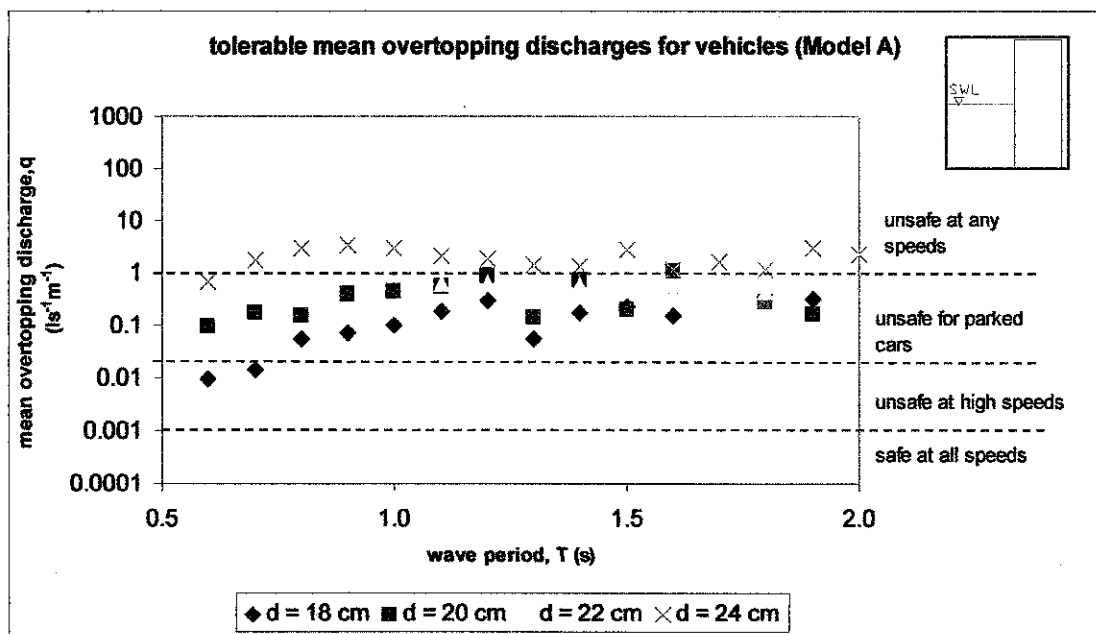*Figure 5.13: Tolerable overtopping rates for vehicles (Model A)*

The summarize risk level with respect to different water depths at 0.5 s $< T < 2.0$ s is presented in Table 5.10. The govern risk level for $d = 18$, 20 and 22 cm is unsafe for parked car which means the wave overtopping could damaged the parked car nearby. As for moving vehicles, it is still safe to move with low speeds. Moving with high speeds

will be unsafe. When $d = 24$ cm, the vehicles will be unsafe at any speed. This could either cause accident or damages to vehicles.

Table 5.10: Risk level for vehicles (Model A)

Water depth, d (cm)	Risk level
18	Unsafe for parked car
20	Unsafe for parked car
22	Unsafe for parked car
24	Unsafe at any speed

For Model B, the tolerable overtopping rates for vehicles are shown in Figure 5.14. As expected, the overtopping rates for $d = 18$ cm were in the unsafe for parked cars zone except for one overtopping rate when the time period was 1.3 s was in unsafe at high speeds zone. All overtopping rates of $d = 20$ cm were in unsafe for parked cars zone. As for $d = 22$ cm, the overtopping rates were in the unsafe for parked cars zone except for overtopping rates at 0.8, 0.9, 1.0, 1.2, 1.4 and 1.5 s. When $d = 24$ cm, most of the overtopping rates were in unsafe at any speed zone except for overtopping rates at 0.6 and 1.8 s.
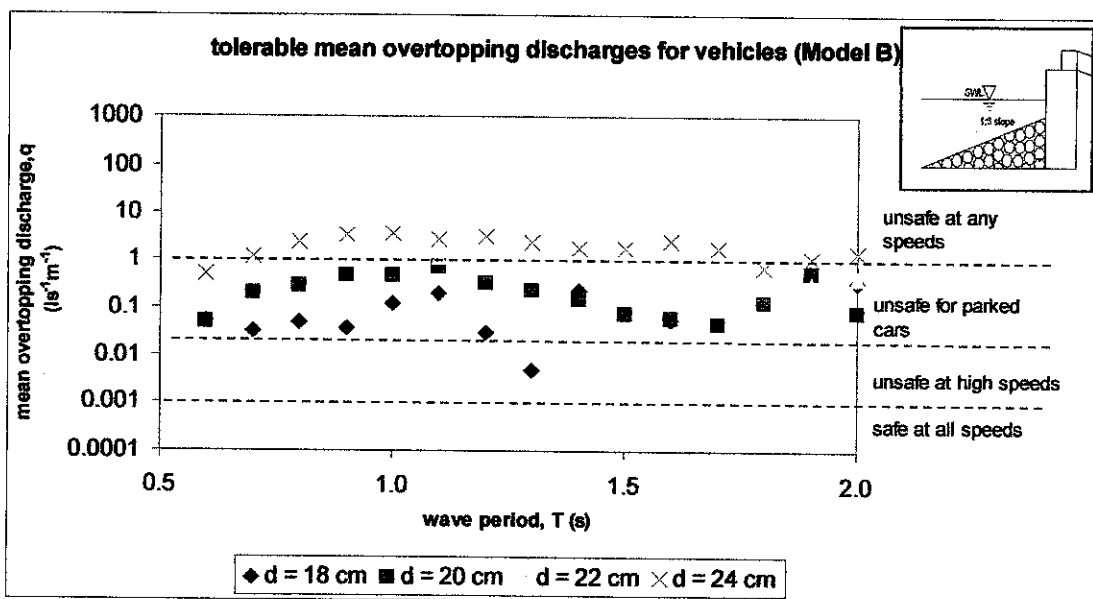

Figure 5.14: Tolerable overtopping rates for vehicles (Model B)

Table 5.11 shows the summarize risk level for each water depth for Model B. The risk level presented in the table is similar to Model A (Table 5.4). Hence, the implications will be on parked cars where it is unsafe when d = 18, 20 and 22 cm and the vehicles are unsafe at any speed for d = 24 cm.

Table 5.11: Risk level for vehicles (Model B)

Water depth, d (cm)	Risk level
18	Unsafe for parked car
20	Unsafe for parked car
22	Unsafe for parked car
24	Unsafe at any speed

The tolerable overtopping rates for Model C were represented in Figure 5.15. In the unsafe at high speeds zone, there were five overtopping rate of d = 18 cm at time period of 0.6, 1.0, 1.3, 1.5 and 1.6 s and an overtopping rate of d = 22 cm at 1.0 s. The remaining overtopping rates for d = 22 cm and overtopping rates for d = 20 cm were in unsafe for parked cars zone. Two overtopping rates of 0.6 and 0.7 s for d = 24 cm were in the unsafe for parked cars zone while the remaining overtopping rates were in unsafe at any speed zone.

The risk level for Model C is also similar to Model A. for d = 18, 20 and 22 cm, it is unsafe for parked car nearby and for d = 24 cm, it is unsafe for vehicles at any speeds. Table 5.12 shows the related risk level for Model C.

Table 5.12: Risk level for vehicles (Model C)

Water depth, d (cm)	Risk level
18	Unsafe for parked car
20	Unsafe for parked car
22	Unsafe for parked car
24	Unsafe at any speed
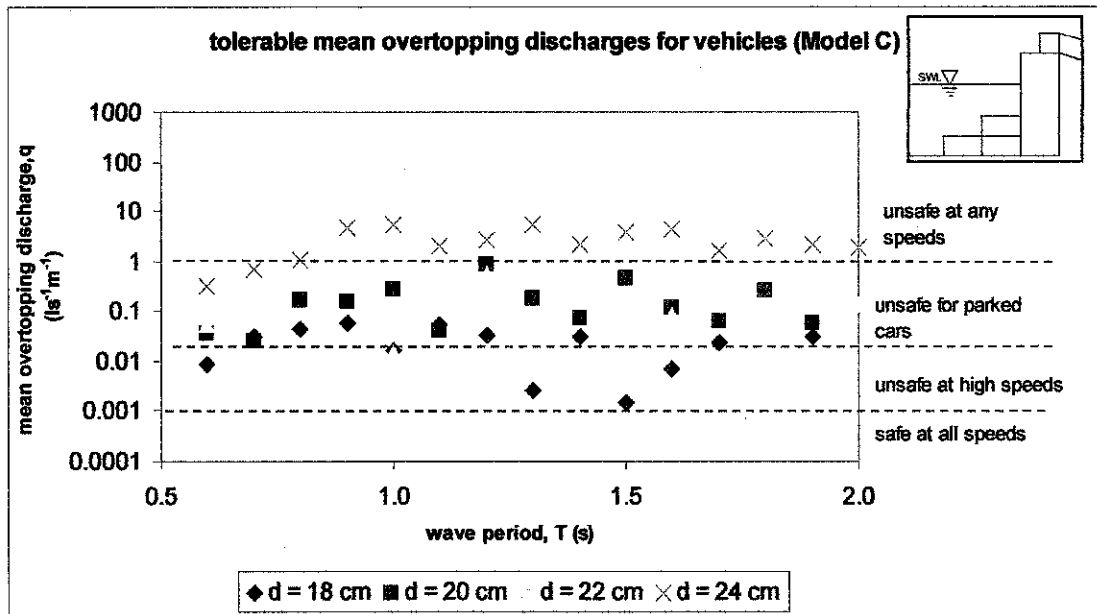
Figure 5.15: Tolerable overtopping rates for vehicles (Model C)

5.5.3 Buildings

For buildings category, the limits were divided into three zones which were no damage, minor damage to fittings etc and structural damage zone. First, the tolerable overtopping rates on buildings for Model A were discussed. As illustrated in Figure 5.16, all the overtopping rates for all water depths were in the structural damage zone except for two overtopping rates of d = 18 cm at 0.6 and 0.7s. The two overtopping rates were in the minor damage zone.

Majority the wave overtopping for each water depth would cause structural damage to buildings behind the seawall which indicate that the situation is dangerous. The risk level is presented in Table 5.13.

Figure 5.16: Tolerable overtopping rates for buildings (Model A)

Table 5.13: Risk level for buildings (Model A)

Water depth, d (cm)	Risk level
18	Structural damage
20	Structural damage
22	Structural damage
24	Structural damage

For model B, most of the overtopping rates were also in the structural damage zone for all water depths except for two overtopping rates at 1.3 and 1.4 s for $d = 18$ cm that fell into minor damage zone. The overtopping rates were almost in the same range as Model A as discussed in previous section. The zones are shown in Figure 5.17 and the summarize risk level is presented in Table 5.14.
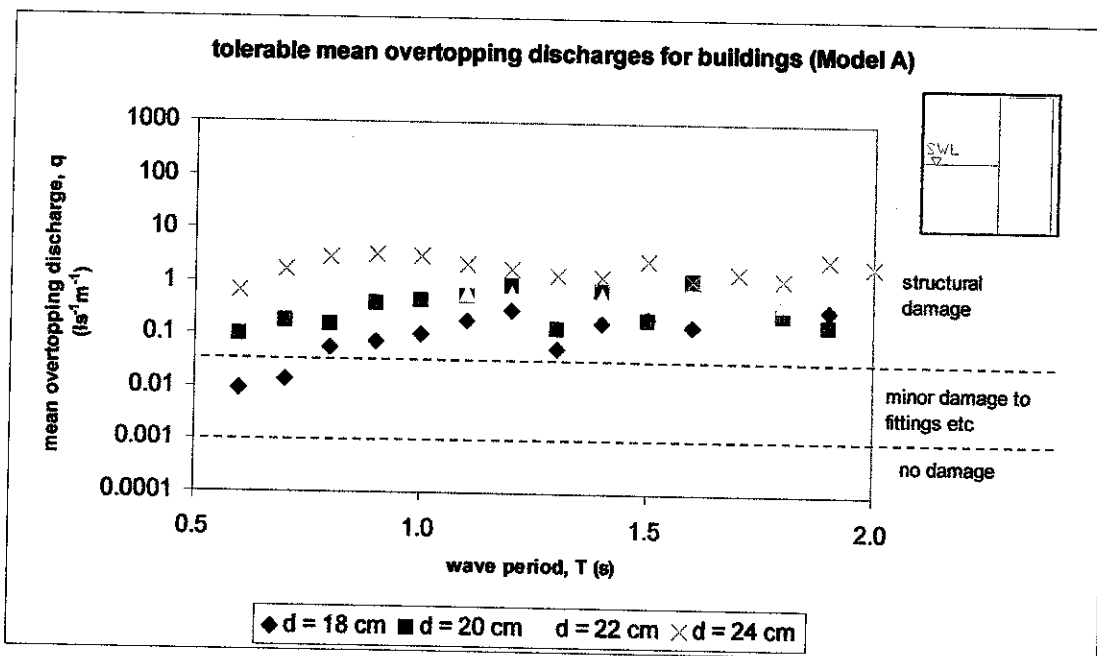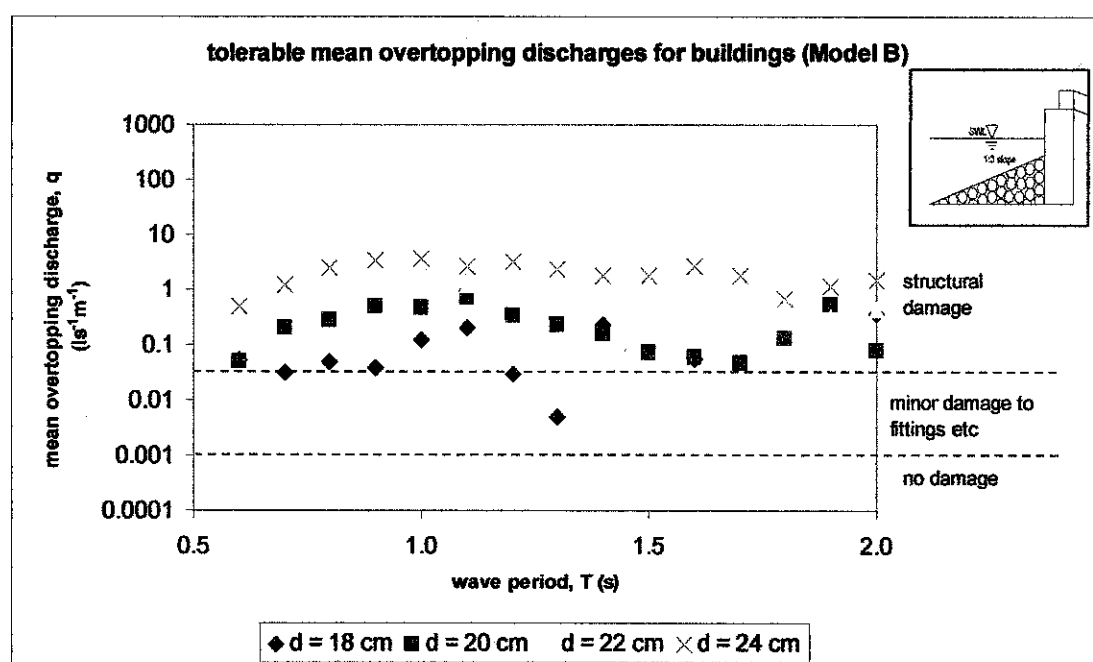
Figure 5.17: Tolerable overtopping rates for buildings (Model B)

Table 5.14: Risk level for buildings (Model B)

Water depth, d (cm)	Risk level
18	Structural damage
20	Structural damage
22	Structural damage
24	Structural damage

It is observed from Figure 5.18 that most of the overtopping rates for $d = 18$ cm were in the minor damage zone for Model C except for overtopping rate at 0.7, 0.8, 0.9 and 1.1 s that fell in the structural damage zone. For $d = 22$ cm at 1.0 s, and $d = 20$ cm at 0.7 s the overtopping rate was in minor damage zone while the remaining rates were in the structural damage zone. All overtopping rates for $d = 24$ cm were in the structural damage zone.

62
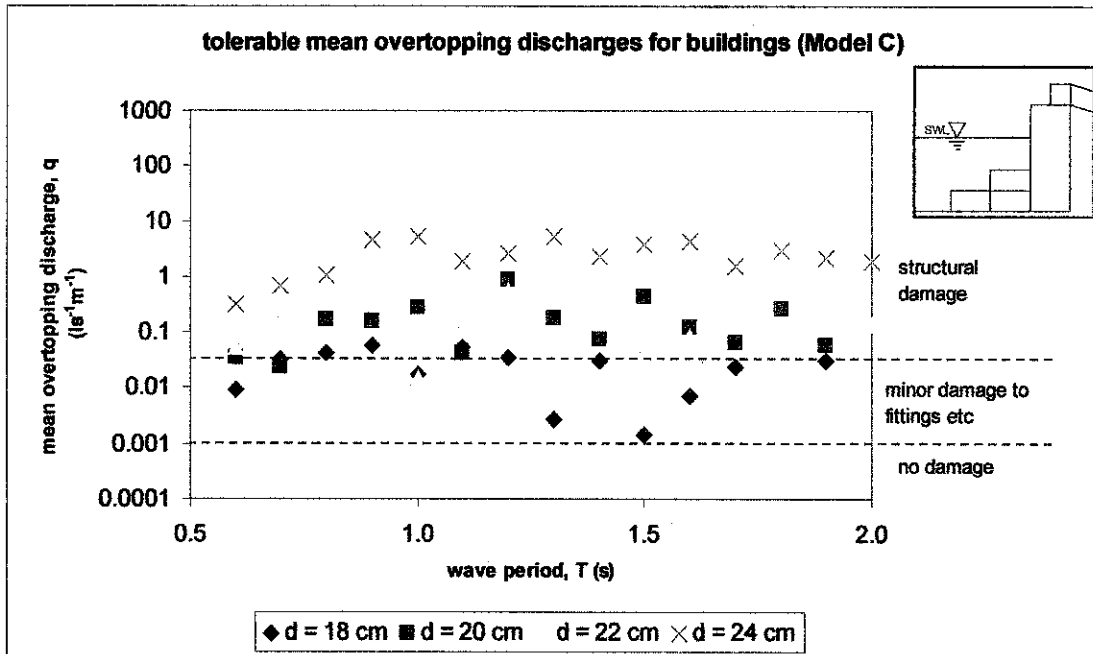
Figure 5.18: Tolerable overtopping rates for buildings (Model C)

The risk level for Model C is presented in Table 5.15. For d = 18 cm, the wave overtopping could only cause minor damage to fittings. This is not a major harm to structures but still need to be taken care of. The minor damage could cause major damage such as structural damage if the water depths increase.

Table 5.15: Risk level for buildings (Model C)

Water depth, d (cm)	Risk level
18	Minor damage to fittings
20	Structural damage
22	Structural damage
24	Structural damage

5.5.4 Embankment Seawalls

It is important to consider the risk of wave overtopping to embankment seawalls since the structures were the main concern in this research. If the structures fail, it could cause hazards to the hinterland.

The govern risk levels for embankment seawalls are no damage, damage if back slope not protected and damage even if fully protected. Graph on the discussed matter for Model A is shown in Figure 5.19.
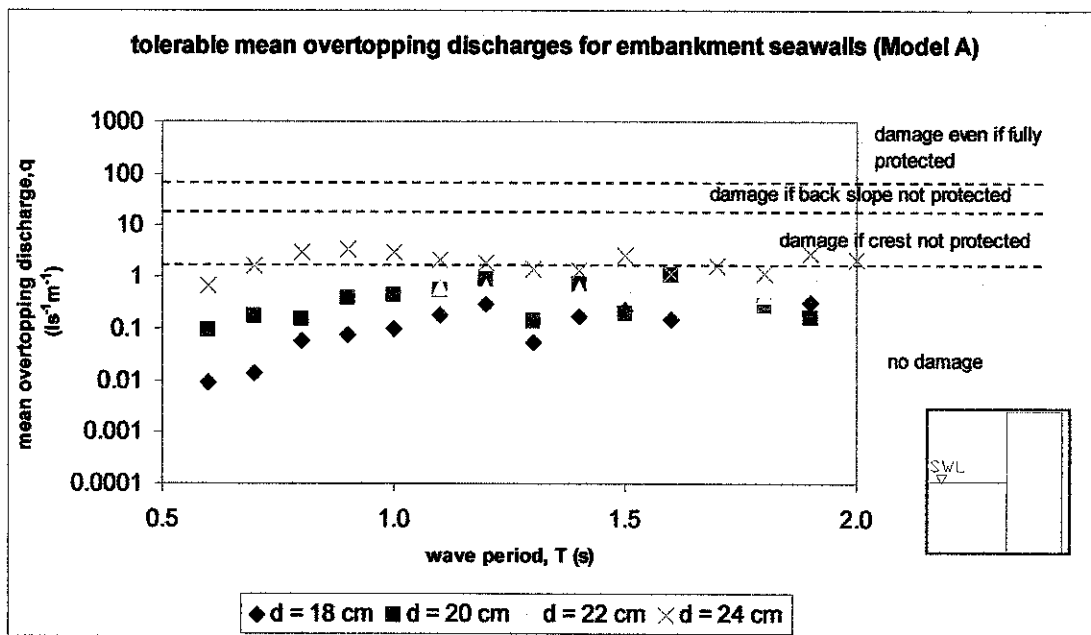
Figure 5.19: Tolerable overtopping rates for embankment seawalls (Model A)

From the figure, the overtopping rates for d = 18, 20 and 22 cm were in the no damage level. As for d = 24 cm, when T = 0.8, 0.9, 1.0, 1.1, 1.5 and 1.9 s, the overtopping rates were in damage if crest not protected while the remaining overtopping rates were in the no damage level. The summarize risk level for each water depth is presented in Table 5.16. For d = 18, 20 and 22 cm, the risk level for embankment seawalls is no damage and for d = 24 cm, the risk level is damage if crest not protected.

Table 5.16: Risk level for embankment seawalls (Model A)

Water depth, d (cm)	Risk level
18	No damage
20	No damage
22	No damage
24	Damage if crest not protected

Figure 5.20 shows the tolerable overtopping rates for embankment seawalls of Model B. Majority of the overtopping rates for d = 18, 20 and 22 cm fell in no damage level. While for d = 24 cm, the overtopping rates were in the damage if crest not protected level when T = 0.7, 0.8, 0.9, 1.0, 1.1, 1.2, 1.3 and 1.6 s. The summarize risk level for each water depth is presented in Table 5.17.

Figure 5.20: Tolerable overtopping rates for embankment seawalls (Model B)

Table 5.17: Risk level for embankment seawalls (Model B)

Water depth, d (cm)	Risk level
18	No damage
20	No damage
22	No damage
24	Damage if crest not protected

Graph of tolerable overtopping rates for embankment seawalls of Model C is as in Figure 5.21. It is observed that overtopping rates for d = 18, 20 and 22 cm were in no damage level as well as d = 24 cm when T = 0.6, 0.7, 0.8, 1.7 and 2.0 s. The remaining overtopping rates for d = 24 cm were in damage if crest not protected level. The summarize risk level is presented in Table 5.18.
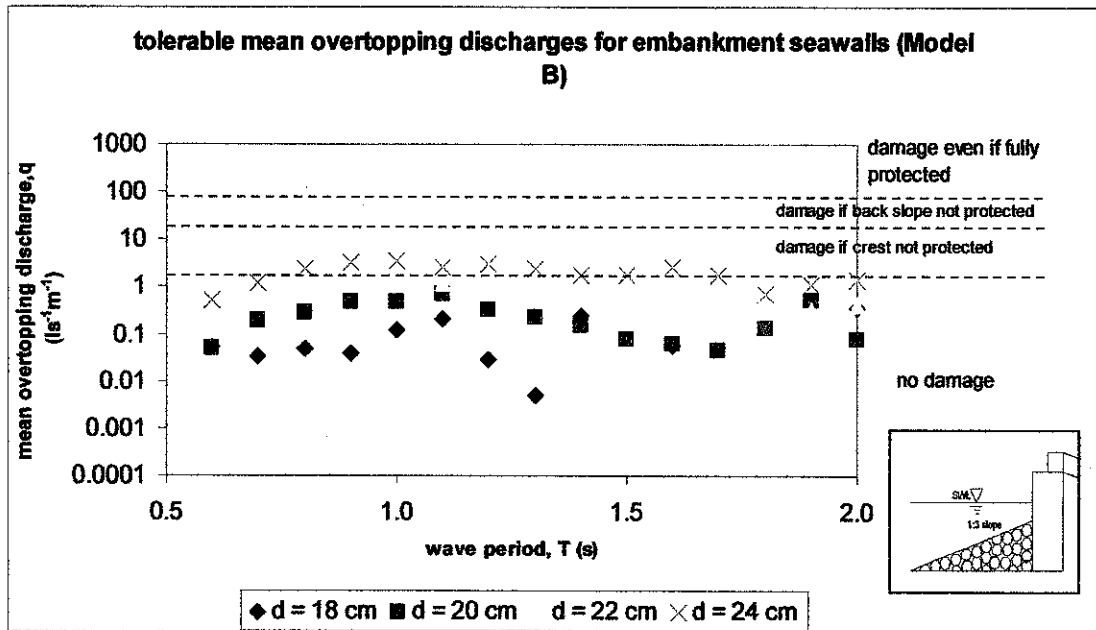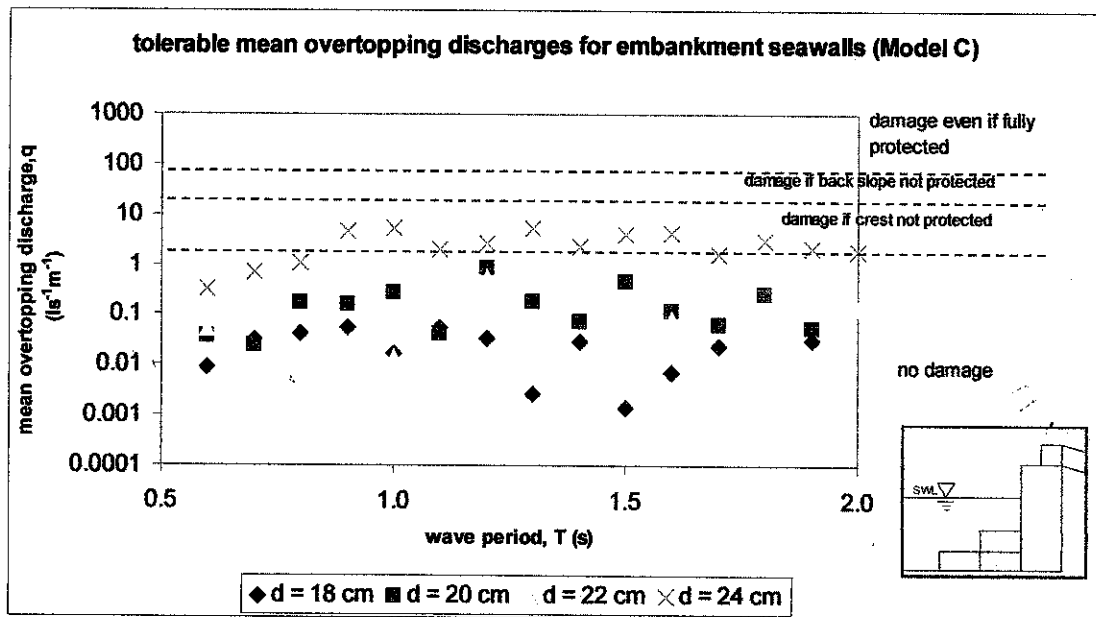

Figure 5.21: Tolerable overtopping rates for embankment seawalls (Model C)

Table 5.18: Risk level for embankment seawalls (Model C)

Water depth, d (cm)	Risk level
18	No damage
20	No damage
22	No damage
24	Damage if crest not protected

From the risk assessment for embankment seawalls discussed previously, it can be observed that for Model A, B and C, for d = 18, 20 and 22 cm the embankment seawalls will not having any damage. However, for d = 24 cm, the seawalls will be damaged if crest is not protected. The damage is not very severe since it still can be repaired without reconstruction.

From the assessment of tolerable overtopping rates on pedestrians, vehicles, buildings and embankment seawalls, it can be said that the wave overtopping values in this research had a major implication to the aspects respectively. Referring to pedestrians, the risk level is most likely fell into dangerous level for Model A, B and C. While for vehicles, the waves overtopping cause an unsafe situation for parked car. In the risk assessment for buildings, the major implication for each model is structural damage which is the highest risk level for buildings. Nevertheless, the waves overtopping did not cause any damage to embankment seawalls.

CHAPTER 6

CONCLUSION AND RECOMMENDATION

6.1   CONCLUSION

1. Two models of composite type seawalls had been identified and studied. They were seawall with quarrystones as armour units and seawall with concrete cubes as armour unit.

2. The models were constructed on a scale of 1:15 using mortar concrete for the vertical wall and concrete cubes. The quarrystones were form the quarry.

3. The experiment were done for three models of seawalls which were vertical seawall (Model A), composite seawall with quarrystones as armour units (Model B) and composite seawall with concrete cubes as armour units (Model C). Model A was for control purposed. The experiments involved were determination of wave period and incident wave height with respect to the wave period. Then the determination of overtopping rates was conducted and the analyses on hydraulics parameters were done followed by risk assessment for pedestrians, vehicles, buildings and embankment seawalls.

4. The tests results show that the wave period depends on frequency and is inversely proportional to frequency. Besides, incident wave height will form a polynomial curve with respect to increasing wave period.

5. Apart from that, the influences of wave steepness and incident wave height on wave overtopping rate were assessed for three seawall models. It can be concluded that the incident wave heights had major influence to overtopping rates. The wave overtopping rate increased with an increased of incident wave height and formed exponential correlations. Water depths also a major parameter

that influenced the overtopping rate of the seawalls where deep water with high waves produce high amount of overtopping volume.

6. From the discussion of tolerable overtopping rates of pedestrians, most of the rates for each model were in the dangerous zone which could cause the pedestrians fall from the walkway and injured. For vehicles, most of the rates for each model were in the unsafe for parked car zone and for buildings most of the rates for each model were in the structural damage zone. As for embankment seawalls, the overtopping rates were most in the no damage zone. These indicated that the overtopping rates were high and hazardous to pedestrians, vehicles and buildings. However, comparing the three models, Model C was the composite type seawall that can reduce overtopping rates better than Model A and B.

6.2   RECOMMENDATION

A few recommendations can be made in order to improve the study:

1. The scope of the study can be expanded by considering the influences of other parameters such as surf similarity, overtopping energy and factor of roughness.

2. The determination of wave overtopping rate can be improved using gauges that can automatically read the rates during experiment.

3. The research can be expanded by studying the seawalls structural parameters such as crest width and slope of armour units to make it less hazardous.

4. The experimental study can be improved by using wave probe in determining incident wave height to prevent human error during the data recording.

5. The study also can be further expanded by experimentally tested other type of composite seawalls design.

REFERENCES

Allsop, N. W. H. (1998). "Hydraulic Performance and Stability of Coastal Structures". In Concrete in Coastal Structures. Thomas Telford Ltd, London. pp. 37-71.

Allsop, N. W. H., Bruce, T., Pearson, J., Alderson, J. and Pullen, T. (2005). " Violent Overtopping at The Coast, When Are We Safe?". London.

Allsop, N. W. H., Bruce, T., Pearson. J. and Besley, P. (2005). "Wave Overtopping at Vertical and Steep Seawalls". Proceedings of the Instituition od Civil Engineers. London.

Bradbury, A.P. and Allsop, N. W. H. (1988). "Hydraulic Effects of Breakwater Crownwalls". Proceedings Conference on Design of Breakwaters. Institution of Civil Engineers. London.

Bruun, P. (1972) "The History and Philosophy of Coastal Protection". In Proceedings Coastal Eng. Conference, Vancouver, Canada. ASCE. pp. 33-74.

CIRIA (1991). "Manual on The Use of Rock in Coastal and Shoreline Engineering". CIRIA Special Publication 83/CUR Report 154. CIRIA. London.

Civil Engineering Department, the Government of Hong Kong Special Administrative Region. (2003). "Guide to Design of Seawalls and Breakwaters". Port Works Design Manual Part 4. pp. 13-15.

Franco, L., de Gerloni, M. and van der Meer, J.W. (1994). "Wave Overtopping on Vertical and Composite Breakwaters". Proceedings 24th ICCE, Kobe. ASCE, New York.

Hughes, S. A. (1995) "Physical Models and Laboratory Techniques in Coastal Engineering". Advance Series on Ocean Engineering. Vol. 7. World Scientific Publishing Co. Pte. Ltd. London.

Jakobsen, K. P. & Frigaard, P. (1999). "User's Manual for the Program Wave Dragon – Power Simulation". CRAFT program Low-Pressure Turbine and Control Equipment for Wave Energy Converters (Wave Dragon). Hydraulics & Coastal Engineering Laboratory, Aalborg University.

Kimura, K., Fujiike, T., Kamikubo, K., Abe, R. and Ishimoto, K. (2000). "Damage to Vehicles on a Coastal Highway by Wave Action". Proceedings of the International Conference on Coastal Structures '99. Ed. Losada, I.J. Santander, Spain. Balkema, Rotterdam, Brookfield Vol. 2, pp. 1009-1016.

Kobayashi, N. and De los Sontos, F. J. (2007)."Irregular Wave Seepage and Overtopping of Permeable Slopes". Journal of Waterway, Port, Coastal, and Ocean Engineering. ASCE.

Kofoed, J. P. and Burcharth, H. F. (2000). "Experimental Verification of an Empirical Model for Time Variation of Overtopping Discharge". <http://www.emu-consult.dk/includes/kofoed_burcharth_dec_2000.pdf>.

Madurini, L. and Allsop, N. W. H. (1995). "Overtopping Performance of Vertical and Composite Breakwaters and Seawalls : Results of Wave Flume Tests". In Proceedings of Final MCS Workshop, Alderney. University of Hanover.

Pilarczyk, K. W. (1990). "Coastal Protection". Proceedings of the Short Course on Coastal Protection, Delft University of Technology. pp. 197-286.

Shankar, N.J. and Jayaratne, M.P.R. (2002). "Wave Run-up and Overtopping on Smooth and Rough Slopes of Coastal Structures". Ocean Engineering 30. pp. 221-238.

Van der Meer, J.W. (1998). "Wave Run-Up and Overtopping". In Dikes and Revetments Design, Maintenance and Safety Assessment. Ed. Pilarczyk, K. W.. A. A. Balkema, Rotterdam, Brookfield. Ch. 8, pp. 145-159.

Van der Meer, J.W. and Janssen, J.P.F.M. (1995). "Wave Run-Up and Overtopping at Dikes". In Wave Forces on Inclined and Vertical Wall Structures. Ed. Kobayashi, N. and Demirbilek, Z. Ch. 1. ASCE. New York.